

**MULTI-SCALE STUDY OF THE DYNAMICS OF SELF-ORGANISING  
MOLECULAR SYSTEMS**

**By  
GÖKHAN KAÇAR**

**Submitted to the Graduate School of Engineering and Natural Sciences  
in partial fulfillment of  
the requirements for the degree of  
Master of Science**

**Sabancı University  
Fall 2008**

**MULTI-SCALE STUDY OF THE DYNAMICS OF SELF-ORGANISING  
MOLECULAR SYSTEMS**

**APPROVED BY:**

Prof. Dr. Canan Atılğan (Thesis Advisor)



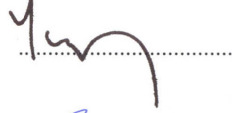
Dr. Alimet Sema Özen (Thesis Co-Advisor)



Prof. Dr. Viktorya Aviyente



Prof. Dr. Yusuf Mencilođlu



Asst. Prof. Dr. Burç Mısırlıođlu



**DATE OF APPROVAL:** ..30/01/2009...

© Gökhan Kaçar 2009

All Rights Reserved

## ABSTRACT

Many research groups are studying self-assembly structures via using computational techniques to understand their behavior from a theoretical point of view. Taking different length scales into consideration becomes more important day by day. In this thesis, calculations are performed at the different length scales of meso-scale, quantum scale, and nano-scale. First of all, meso-scale calculations are performed by using the Dissipative Particle Dynamics simulation methodology to obtain the three dimensional morphologies and the corresponding equilibrium structures. These structures are obtained as a collection of beads each of which consists of several atoms. Hence, morphologies varying from spherical and cylindrical micellar to lamellar are obtained. Then, in order to understand origins of interactions between beads forming meso-scale morphologies, quantum mechanical calculations are carried out at the nano-scale by using chemical reactivities and Atoms-In-Molecules theory. The interactions that occur on the interatomic scale are found to control the meso-scale. In addition to meso-scale calculations to obtain morphology, micelles are investigated in terms of their surface-to-volume ratios to the micro-phase separation behavior. Consequently, phase change from spherical to cylindrical micellar and micellar to lamellar phase is observed in surface-to-volume versus concentration plot. Finally, molecular dynamics simulations on the atomic scale are performed to study the dynamics of self-assembled synthetic structures. A reverse mapping algorithm is developed to back fit atomistic detail to morphologies obtained from meso-scale calculations. The detailed structure is soaked into water to study the dynamics of interfacial water since the target structure is superhydrophobic.

## ÖZET

Kendine kendine örgütlenen sistemler günümüzde birçok araştırmacı tarafından hesaplamalı teknikler kullanılarak teorik olarak çalışılmaktadır. Değişik uzunluk mertebelerini hesaba katmak gün geçtikçe daha çok önem kazanmaktadır. Bu çalışmada, meso-ölçek, nano-ölçek ve kuantum ölçekleri olmak üzere değişik uzunluk ölçüleri kullanılarak hesaplamalar yapılmıştır. Başlangıç olarak, Dağılıcı Parçacık Dinamiği benzetim yöntemi kullanılarak meso-ölçekte hesaplamalar yapılmış, üç boyutlu morfolojiler ve denge halindeki yapılar elde edilmiştir. Bu yapılar, çeşitli sayıda atomun bir araya gelmesinden oluşan tanecikler cinsinden elde edilmektedir. Sonuç olarak, elde edilen yapılar küresel, silindirik miseller ve lameller olarak gözlemlenmiştir. Buna ek olarak, meso-ölçekteki morfolojileri oluşturan etkileşimlerin daha iyi anlaşılması için kuantum ölçek hesapları, kimyasal reaktivite ve Moleküller İçindeki Atomlar teorisi kullanılarak gerçekleştirilmiştir. Atomlararası ölçekteki etkileşimlerin, meso-ölçekteki morfolojileri etkilediği gözlemlenmiştir. Morfoloji elde etmek için gerçekleştirilen hesaplara ek olarak, misellerin mikro-faz ayırma karakterinin belirlenmesi için misellerin yüzey alanı-hacim oranları çıkarılmıştır. Sonuç olarak, yüzey alanı-hacim oranı ve oligomer konsantrasyon grafiğinde, küreselden silindirik misele ve misel yapıdan lamele faz geçişleri gözlemlenmiştir. Son çalışma olarak, atomik ölçekteki moleküler dinamik benzetim yöntemi, kendi kendine örgütlenen bu sentetik sistemlerin dinamiğinin çalışılması için kullanılacaktır. Atomik detay geri kazandırma algoritması geliştirilmiş ve meso-ölçekte elde edilen morfolojilere uygulanmıştır. Morfolojileri elde etmek için kullanılan yapı su sevmeyen karakterde olduğu için, atomik detayı geri kazandırılmış sistem, ara-yüzeydeki suyun dinamiklerini incelemek üzere suya batırılmıştır.

*“To my family”*

## ACKNOWLEDGEMENTS

It is a great pleasure to work under supervision of Prof. Canan Atılgan. I would like to express my deepest gratitude to my thesis advisor for her invaluable guidance, motivation and endless encouragement throughout this study. I will always be thankful to her advices that made me a better researcher and a better person. I would not be in this point without her support.

I would also like to thank to my Co-Advisor Dr. Alimet Sema Özen for her moral support and invaluable ideas that opened very interesting areas to explore throughout my thesis work.

I also want to express my thanks to Prof. Ali Rana Atılgan for the very helpful discussions during my thesis studies. This thesis would be incomplete without his support.

I also would like to send my thanks to the thesis committee: Prof. Viktorya Aviyente, Prof. Yusuf Mencilođlu, Assist. Prof. Burç Mısırlıođlu for their invaluable comments and review on the thesis.

I want to thank Assist. Prof. Mehmet Yıldız for his suggestions on reading and commenting on my thesis.

All of my friends made me have a great working time in Sabanci University. I specially thank Computational Lab members; Murat Mülâyım, Özlem Aykut, Deniz Turgut, İbrahim İnaç, Osman Burak Okan and MAT Grad. students; Koray Aras, Can Kartođlu, Cahit Dalgıçtır, Emre Fırlar, Firuze Okyay, Zuhâl Taşdemir, Eren Şimşek, Özge Malay, Vanya Anna Uluç, Seren Yüksel, Gülay Bozoklu and the rest, and also to my friends from BIO Grads. Ebru Kaymak, Emel Yeşil, Aydın Albayrak, Simin Ataç, İzzet Akiva for their friendship and support.

Finally, I would like to acknowledge Turkish Scientific and Technological Research Council (TUBITAK) for supporting this thesis.

## TABLE OF CONTENTS

ABSTRACT.....	iv
ÖZET .....	v
ACKNOWLEDGEMENTS .....	vii
TABLE OF CONTENTS.....	viii
LIST OF TABLES .....	x
LIST OF FIGURES .....	xi
1. INTRODUCTION .....	1
2. MATERIALS AND METHODS .....	5
2.1. Computational Methods .....	5
2.1.1. Dissipative Particle Dynamics (DPD) Simulation Method .....	5
2.1.1.1. Parametrization Details for Systems Studied .....	7
2.1.2. Quantum Mechanical (QM) Calculations.....	8
2.1.3. Molecular Dynamics (MD) Simulations.....	11
2.1.4. Minimization Methods.....	12
2.1.5. COMPASS Force Field .....	13
2.2. Systems Studied .....	14
2.2.1. Fluorinated Block Co-Oligomer Systems.....	14
2.2.1.1. System Formation for Simulations.....	14
2.2.2. Surfactant Systems.....	15
2.3. Atomistic Detail Reverse Mapping Algorithm .....	17
2.4. Calculating the realistic length scales of the DPD systems .....	21
3. RESULTS AND DISCUSSION.....	23
3.1. DPD Simulations.....	23
3.1.1. Fluorinated Co-Oligomer Systems .....	23
3.1.1.1. Styrene-co-PFA System .....	23

3.1.1.2.	MMA-co-PFA System.....	25
3.2.	Quantum Mechanical Calculations .....	27
3.2.1.	Styrene-co-PFA Oligomer System .....	27
3.2.2.	MMA-co-PFA Oligomer System.....	29
3.3.	Surfactant System.....	30
3.4.	Reverse Mapping of Atomistic Detail.....	37
4.	CONCLUSIONS AND RECOMMENDATIONS FOR FUTURE STUDIES .....	41
5.	REFERENCES .....	44

## LIST OF TABLES

Table 2-1. Amount and type of beads with corresponding molecular structures in one box. ....	21
Table 3-1. Interaction parameters ( $a_{ij}$ ) of fluorinated Styrene-co-PFA system (in $k_B T$ units). ....	23
Table 3-2. Interaction parameters ( $a_{ij}$ ) of fluorinated MMA-co-PFA system (in $kT$ units). ....	25
Table 3-3. Chemical reactivity values calculated for ring center on MP2/6-31G(d) level and solubility parameters for Styrene-co-PFA oligomer system. ....	28
Table 3-4. Chemical reactivity values calculated on MP2/6-31G(d) level and solubility parameters for MMA-co-PFA oligomer system. ....	30
Table 3-5. Interaction parameters ( $a_{ij}$ ) of the compounds 1-9 (in $kT$ units); also listed are the bead molar volumes.* ....	31

## LIST OF FIGURES

Figure 2-1. (a) Styrene-co-PFA and (b) Methylmethacrylate-co-PFA co-polymers (c) Tetrahydrofuran (THF) as solvent. ....	15
Figure 2-2. Molecular structures of ABCBA type model surfactant oligomer, with the nine different types of R groups in the CO <sub>2</sub> -phobic segment. ....	16
Figure 2-3. Center of masses of molecules are translated to coordinates of beads. The A <sub>10</sub> B <sub>1</sub> D <sub>7</sub> system is shown schematically (see section 2.2.1.1) black, red and blue dots are styrene, hydrophobic part of PFA and fluorinated part of PFA, respectively. ....	17
Figure 2-4. Projection onto the <i>x-z</i> plane. ....	18
Figure 2-5. Distance vectors between consecutive templates. ....	20
Figure 2-6. Scale factor of a DPD unit is determined by selecting minimum RMSD value of two conformations of a styrene-co-PFA chain (circle). ....	22
Figure 3-1. Mesoscopic morphologies obtained due to various molar compositions of Styrene-co-PFA oligomers in THF solvent. ....	24
Figure 3-2. Mesoscopic morphologies obtained due to various molar compositions of MMA-co-PFA oligomers in THF solvent. ....	26
Figure 3-3. Interaction energy of styrene (a) on the same chain is 3.5 kcal/mol and (b) on different chains is 1.5-2.0 kcal/mol. Yellow, purple and blue dots show ring, bond and cage critical points, respectively. ....	29
Figure 3-4. Morphologies obtained with respect to different type of side chains. ....	33
Figure 3-5. Surface area-volume ratios (S/V) of micelles changing with respect to volume concentration of the oligomer. ....	34
Figure 3-6. Variation in the radial distribution functions, <i>g(r)</i> , of beads in the system with oligomer concentration. (a) Total distribution of beads in the system does not change. The pressure, however, monotonically decreases with increasing concentration (inset). Intermolecular number density distribution of beads decreases with concentration (b), whereas intramolecular distribution increases. ....	35

Figure 3-7. Morphologies obtained after applying (a) shear rate 0.001 and (b) shear rate 0.01. ....	36
Figure 3-8. Atomistic detailed single Styrene-co-PFA oligomer chain structures obtained after (a) Translation, (b) Rotation and (c) Energy minimized. ....	38
Figure 3-9. Spherical morphology of 10 % styrene-co-PFA oligomer system (a) consisting of beads, (b) after atomistic detail is reverse mapped. ....	39
Figure 3-10. Atomistic detail reverse mapped styrene-co-PFA oligomer soaked into water box.....	39

## 1. INTRODUCTION

After Taniguchi first used the word “nanotechnology,” it has become one of the most widely studied scientific subjects in the past few decades [1]. Many research groups work on designing and developing brand-new materials that have high economic importance by using methods based on or derived from nanotechnology. Designing new materials requires a good understanding of their structure-property relationships at different length and time scales ranging from nano to micro or to macro. Mono-scale approaches of computational science are inadequate to understand the structure-property relationship; multi-scale approaches can be more useful to attain this goal in terms of bridging gaps between these scales.

Studies on modeling self-organizing macromolecular systems at many scales have been drawing attention of very wide range of researchers in the last years [2, 3]. Among these computational techniques, molecular dynamics (MD) methods [4, 5] are very useful in terms of generating time and length evolution of a self-assembly system. For example; proteins are considered as “self-organizing” polymers and it is known that they fold into their native structure at millisecond or longer time scales. Dynamics around the folded state in terms of fluctuations give function to these self-assembly structures and molecular dynamics (MD) techniques are being used widely to predict these dynamics [4, 6]. So, in order to study these fluctuations, average structures in their native state need to be known. They are derived from experimental sources and deposited in the Protein Data Bank [7].

The crucial limitation of the MD techniques is the real computational time that allows the runs at the time scales of interest. With the current available computers, one can only simulate tens of nanoseconds, but for synthetic self-organized molecular systems, this time scale extends to the order of millisecond to seconds in order to evolve to the self-organized state. In addition, there is no experimental atomistic coordinate depository for synthetic self-organized systems. Researchers resort to coarse-grained simulation techniques [8, 9] to predict their average equilibrium structures. In these coarse-grained techniques, the system under study loses its atomistic detail as the atoms constituting the system are gathered into beads that are assumed to interact with each

other. The interaction parameters are based on physical principles and are derived from atomistic details of the beads.

Groot and Warren have developed Dissipative Particle Dynamics (DPD) method [10] to obtain polymer morphologies. Interaction parameters are based on solubility parameters that were acquired from MD simulations. The morphologies obtained by this method are consistent with experimental results [10]. The crucial property in their work is that they use averages of the atomistic properties in calculating interaction parameters and thereby coarse graining the atomistic details for multi-scale simulations to reach higher length and time scales. According to their methodology, interaction parameters are calculated based on Flory-Huggins theory [10, 11].

In this method, Newton's equations of motion are the bases for movement of the particles in the system [12]. DPD method is known as successfully bridging gap between microscopic simulation methods and the macroscopic approaches.

Utilization of DPD to obtain morphologies has a very wide range of applications in co-oligomeric systems. For example, mesoscopic morphologies of linear and graft block copolymers are obtained by using DPD method and fluorine-containing groups are found to be immiscible with other parts of the polymer and with the solvent which lead to micellar morphologies [9]. These fluorinated systems are known for their superhydrophobicity, bioinertness and solubility in supercritical carbon dioxide [13].

Self-assembled structures known as surfactants serve for designing and producing nanometer sized structures [14]. They have wide application areas in pharmaceutical, chemical, household, agricultural chemicals and food processing industries [15]. Different morphologies of surfactants are characterized by their structural properties of non-polar or polar segments. They can form morphologies such as rodlike, globular or bilayer [16, 17]. Hence, understanding structural properties, as potential driving forces for the resulting morphologies becomes a very important task.

On the other hand, multi-scale modeling covers a wide methodological approach from quantum mechanics (QM) to the finite element modeling of the macro systems since dynamical processes and structural changes are correlated. Although, coarse-

grained techniques are being used widely at the nano- and meso-scale, they require certain assumptions related to parameterization based on data obtained from experimental results. Besides, chemical reactivity descriptors such as electronegativity [18], electronic chemical potential [19], hardness and softness [20, 21] can be used to obtain general chemical rules that will allow predicting the properties of self-assembly systems. In addition, Density Functional Theory principles such as Pearson's hard and soft acids and bases principle [20, 21], Sanderson's electronegativity equalization principle [22], and maximum hardness principle [20, 21] have served for a better understanding for the intermolecular and intramolecular interactions. There are studies that compose information from both MD and quantum mechanical calculations to derive new information in chemical synthesis of molecules [23].

It is clear that observing dynamics for synthetic self-organizing systems on time scales ranging from milliseconds to seconds at their native state requires very long computational time. Although, mesoscopic simulation techniques are very fundamental in obtaining morphologies, they have a significant limitation that they do not contain atomistic detail. Hence, to study the related dynamics, it is of great importance to have atomistic detail implemented on beads that have been coarse-grained. There are several reverse-mapping strategies to the coarse-grained systems. For example, Santangelo et. al. proposed a fully geometric approach to reverse map atomistic detail to coarse-grained models of vinyl polymers [24]. They built diads which represent different types of vinyl polymers and fit them according to the original structure sequence. Although other algorithms for this purpose have also been developed [25, 26], there is no example of reverse-mapping onto complex systems such as the output obtained by a mesoscopic DPD.

In this work, we study several selected systems on different length scales such as meso-scale, quantum-scale and nano-scale. Fluorine containing oligomers chosen for this work were previously synthesized experimentally [27, 28]. We first derived morphologies by using DPD simulation method [29]. After obtaining morphologies on the meso-scale, systems are studied at different length scales. First, for a better understanding of the self-assembly properties of these systems, quantum mechanical calculations are carried out [30]. Chemical reactivity indices such as local hardness are calculated for certain parts of the fluorinated co-oligomer system. For surfactant

systems, surface area to volume ratios are calculated to observe the self-assembly and solvation behavior at the meso-scale. Finally, an atomistic reverse mapping algorithm is derived and applied to the simulated systems of morphologies. Atoms constituting coarse-grained beads are fit by taking the coordinates obtained from DPD simulations as bases to obtain initial set of coordinate data to be used as input for MD simulations. Our reverse mapping algorithm differs from the literature as a wide range of possible conformations of molecules that form the beads are considered while searching minimum energy level. Also, more complex systems can be studied with our algorithm with little additional computational time. The ultimate goal is to study the related dynamics for the system of interest.

## 2. MATERIALS AND METHODS

### 2.1. Computational Methods

#### 2.1.1. Dissipative Particle Dynamics (DPD) Simulation Method

DPD simulation method is a tool to simulate the long time scale behavior of complex fluids at the mesoscopic length scale [12, 31]. Systems being simulated are made-up of a collection of coarse-grained beads, each comprised of a collection of atoms. The force on each bead  $i$  is;

$$\mathbf{f}_i = \sum_{j \neq i} (\mathbf{F}_{ij}^C + \mathbf{F}_{ij}^D + \mathbf{F}_{ij}^R) + \sum_k (\mathbf{F}_{ik}^{conn}) \quad (2.1)$$

where  $\mathbf{F}_{ij}^C$ ,  $\mathbf{F}_{ij}^D$  and  $\mathbf{F}_{ij}^R$  are the conservative, dissipative and random forces between the  $i$  and  $j$  beads, respectively.  $\mathbf{F}_{ik}^{conn}$  is the force that represents chain connectivity between bead  $i$  and all beads  $k$ .  $K$  is the spring constant of the springs that connect these beads:

$$\mathbf{F}_{i,k}^{conn} = K\mathbf{r}_{i,k} \quad (2.2)$$

In equation 2.3,  $\mathbf{F}_{ij}^C$  shows the interaction between the beads in the conservative force,

$$\mathbf{F}_{ij}^C = \begin{cases} a_{ij}(1 - r_{ij})\hat{\mathbf{r}}_{ij} & r_{ij} < 1 \\ 0 & r_{ij} \geq 1 \end{cases} \quad (2.3)$$

Here,  $r_{ij}$  is the distance between beads  $i$  and  $j$  normalized by a cut-off distance,  $R_c$ , which defines the distance of interaction.  $\hat{\mathbf{r}}_{ij}$  denotes the unit vector between particles  $i$  and  $j$  and  $a_{ij}$  is the maximum repulsion between particles  $i$  and  $j$ .  $a_{ij}$  parameter gives all

information of the characteristic of interaction and it is based on chemical details of the beads.

$\mathbf{F}_{ij}^D$  is the dissipative force, which acts as a heat sink between beads:

$$\mathbf{F}_{ij}^D = \begin{cases} -\gamma\omega^D(r_{ij})(\hat{\mathbf{r}}_{ij}\cdot\mathbf{v}_{ij})\hat{\mathbf{r}}_{ij} & r_{ij} < 1 \\ 0 & r_{ij} \geq 1 \end{cases} \quad (2.4)$$

where  $\gamma$  is the friction coefficient,  $\omega^D(r_{ij})$  is a short-range weight function and  $\mathbf{v}_{ij}$  is the difference between velocities of the beads  $i$  and  $j$ .

The random force,  $\mathbf{F}_{ij}^R$ , operates as a heat source between moving beads which is computed as:

$$\mathbf{F}_{ij}^R = \begin{cases} \sigma\omega^R(r_{ij})\theta_{ij}\hat{\mathbf{r}}_{ij} & r_{ij} < 1 \\ 0 & r_{ij} \geq 1 \end{cases} \quad (2.5)$$

where  $\omega^R(r_{ij})$  is the distance-dependent weight function that takes zero value at the cut-off distance and  $\theta_{ij}$  is the random fluctuating variable. The weight functions and constants in equations (2.4) and (2.5) are chosen such that the model conserves momentum and gives the correct hydrodynamic behavior [32].

$$[\omega^R(r_{ij})]^2 = \omega^D(r_{ij}) \quad ; \quad \sigma^2 = 2k_B T \gamma \quad (2.6)$$

where  $k_B$  is a Boltzmann constant and  $T$  is the temperature of the fluid. The equations of motion are integrated by a modified velocity-Verlet algorithm [10]. Periodic boundary conditions are employed.

### 2.1.1.1. Parametrization Details for Systems Studied

The interaction term in the conservative force is based on the Flory-Huggins interaction parameter ( $\chi$ -parameter). Groot and Warren performed a series of DPD calculations on binary mixtures with a variety of repulsion parameters [10]. They have found a linear relationship between  $\chi$  and  $a_{ij}$  and this relationship helps to calculate  $\chi$  parameter which is input for DPD simulations. At a given density of  $\rho=3$  relation takes the form;

$$a_{ij} \approx a_{ii} + 3.27\chi_{ij} \quad (2.7)$$

In this equation,  $a_{ii}$  is 25 in units of  $k_B T$ . Values larger than  $25 k_B T$  signify repulsive and those below  $25 k_B T$  signify attractive interactions between beads  $i$  and  $j$ .

In order to calculate Flory-Huggins interaction parameter, solubility parameters ( $\delta$ ) are used from the relation:

$$\chi = \frac{V_m(\delta_i - \delta_j)^2}{RT} \quad (2.8)$$

where,  $V_m$  is the average molar volume of the beads. In the current work we neglect the free volume term in the  $\chi$  parameter since these oligomers have low molecular weight [33]. Molar volumes of beads are calculated by using ACDLabs/ChemSketch 5.0 software [34].

The Amorphous Cell module of Materials Studio 4.3 is used to make atomistic MD simulations to obtain the solubility parameters [29]. COMPASS force field is used in minimization of the system and MD simulations since it has a high accuracy in predicting properties of (see also section 2.1.5) most common organics, inorganic small molecules and polymers [35]. Minimizations are done by consecutive application of Steepest Descent, Conjugate Gradients and Newton minimization methods for 20000 steps [29] (see also section 2.1.4). MD simulations are employed in the canonical ensemble (NVT) and at 298 K and 10 ps MD simulations are been performed. Inside the

simulation boxes, 10 conformations are allowed, and density of 1.0 is satisfied with a cut-off distance value of 8.5 Å.

For both the fluorinated and surfactant systems, DPD simulations are performed to obtain morphologies by using Materials Studio software [29]. Cubic box sizes are selected as 10x10x10 DPD units, so that number of beads in a box will be 6000 after selecting density as 3.0. The only difference between simulations of the fluorine containing system and the surfactant system is the number of DPD time steps. At the end of the simulations 120 000 and 150 000 steps of simulation time is completed for the surfactant and fluorinated system, respectively.

Simulations of these systems are done by using Amorphous Cell, DPD, MS Visualizer, Discover modules in Materials Studio 4.2.0 and Materials Studio 4.3.0 versions of Accelrys Inc. [29]. Computer with an; Intel(R) Core(TM)2 Quad CPU 2.40 GHz processor and system memory (RAM) of 2.00 GB is used to perform simulations. A typical DPD run of 120 000 time steps take fifty minutes of computer time.

### **2.1.2. Quantum Mechanical (QM) Calculations**

For fluorinated co-oligomers, QM calculations are performed in order to understand the molecular basis for self-assembly. The origin of non-covalent interactions that might be essential for self-assembly of the fluorinated structures is investigated by using Atoms-in-Molecules Theory (AIM) Quantum mechanical calculations were performed at the MP2/6-31(d) level.

The AIM theory suggests that a critical point is a point which is a saddle, minimum or a maximum point of an extremum in the electronic density function,  $\rho(r)$ . Number of non-zero eigenvalues or local intrinsic curves (rank,  $\mathbf{r}$ ) and sum of the signs of these eigenvalues (signature,  $\mathbf{s}$ ) defines any critical point ( $\mathbf{r}$ ,  $\mathbf{s}$ ). For instance; a saddle point with three non-zero eigenvalues (rank = 3), which corresponds to maxima in two directions and a minimum in one direction (signature = -1) defines a bond critical point (bcp) which is a saddle point and is represented as (3, -1).

Inter-atomic interactions can be separated into: Shared or Closed-Shell interactions using AIM Theory parameters. Shared interactions such as ionic bonds, hydrogen bonds, bonds in van der Waals molecules and noble gas clusters are one where the Laplacian of electronic density,  $\nabla^2\rho(r)$ , is negative (electron concentration) with a  $\rho(r)$  value of the order  $10^{-1}$  au ( $0.675 \text{ e } \text{\AA}^{-3}$ ). If  $\nabla^2\rho(r)$  is positive (electron depletion) with a  $\rho(r)$  value of the order  $10^{-2}$  au ( $0.068 \text{ e } \text{\AA}^{-3}$ ), then it is a closed-shell interaction [36] like covalent or polar bonds. In addition, relatively high  $\rho(r)$  values with a positive  $\nabla^2\rho(r)$  define intermediate interactions.

In this work, similarity between the subsystems constituting the oligomers, which is considered as a basis for the like-dislike behavior, is also investigated in terms of their electronic structures. For this purpose, local hardness values are calculated. The concepts of local hardness were introduced by Parr [37, 38]. Local hardness,  $\eta$ , basically measures the change in chemical potential with electron density in different parts of the molecule. Local hardness is defined as;

$$\tilde{\eta}(r) = \frac{1}{2} \left( \frac{\delta\mu}{\delta\rho} \right)_v \quad (2.9)$$

Calculation of the exact local hardness is relatively difficult. Therefore there are different approaches for the calculation of local hardness. One of them is Thomas-Fermi-Dirac approach and it introduces the use of the electronic part of the molecular electrostatic potential.

$$\eta_D(r) \approx -\frac{1}{2N} V_{el}(r) \quad (2.10)$$

Also, local softness,  $s$ , is introduced by Yang and Parr [39];

$$s(r) = \left( \frac{\partial\rho(r)}{\partial\mu} \right)_{v(r)} \quad (2.11)$$

as a local analogue of local softness which can be written as;

$$S = \left( \frac{\partial N}{\partial \mu} \right)_{v(r)} \quad (2.12)$$

where  $f$  is the frontier orbital density, called the Fukui Function. Direction of electron flow defines two frontier orbitals. By applying the chain rule,  $s(r)$  can be written as the product of the total softness and the Fukui function,

$$s(r) = \left( \frac{\partial \rho(r)}{\partial N} \right)_v \left( \frac{\partial N}{\partial \mu} \right)_v = \left( \frac{\partial \rho(r)}{\partial \mu} \right)_v = f(r)S \quad (2.13)$$

in which  $f(r)$  redistributes the global softness among the different parts of the molecule and  $s(r)$  integrates to  $S$ :

$$\int s(r)dr = \int Sf(r)dr = S \int f(r)dr = S \quad (2.14)$$

where Fukui function,  $f(r)$ , is defined as the change in electron density,  $\rho(r)$ , at each point  $\mathbf{r}$  when the total number of electrons is changed or as the sensitivity of a system's chemical potential to an external perturbation at a particular point  $\mathbf{r}$ ,

$$f(r) = \left( \frac{\partial \rho(r)}{\partial N} \right)_v = \left( \frac{\delta \mu}{\delta v(r)} \right)_N \quad (2.15)$$

The Fukui function contains relative information about different regions in a given molecule.

$$\begin{aligned} f^-(r) &= \rho_{HOMO}, & \text{electrophilic attack,} \\ f^+(r) &= \rho_{LUMO}, & \text{nucleophilic attack,} \\ f^0 &= \frac{1}{2}(\rho_{HOMO} + \rho_{LUMO}) & \text{radical attack} \end{aligned} \quad (2.16)$$

Local hardness is based on the electronic distribution leading to a net charge on the atom. Local hardness increases with net positive charge [40]. In addition, the closer the local hardness values of two systems, the more two systems resemble each other.

Calculation of energies and geometries are done by using Gaussian 03 software [30]. Ground state structures have been confirmed with frequency analyses. Wave function files were generated with Gaussian 03 program at the level MP2/6-31G(d) prior to the analysis for the electron density contours and topological critical points using the AIM 2000 implementation of Bader's AIMPACK suite of programs [41, 42]. Gaussview software has been used for the graphical representation of the geometries.

### 2.1.3. Molecular Dynamics (MD) Simulations

MD simulations are used to investigate structure-function relationships in materials. Experiments do not usually provide direct molecular level information, however MD allows predicting properties of systems which have not been synthesized or have little structural information.

In MD, structural information are derived by taking Newton's laws of motion as bases for calculations.

$$F_i = ma_i \quad (2.17)$$

where  $F_i$  is the force on the particle,  $m$  is mass and  $a_i$  is the acceleration of particle  $i$ .

Successive system configurations are calculated, so the positions and velocities of the particles in the system vary with time. These trajectories are obtained by solving differential equations of Newton's second law:

$$\frac{d^2 x_i}{dt^2} = \frac{F_{x_i}}{m_i} \quad (2.18)$$

This equation describes the motion of a particle of mass  $m_i$  along one coordinate ( $x_i$ ) with  $F_{xi}$  being the force on the particle in that direction.

Force term is the derivative of the potential with respect to the position of the particle  $i$ . Hence, this potential that characterizes the motion of any particle is the sum of overall interactions and it is called a Forcefield. Since this potential is sum of all interactions that is integrated over all particles in the system, finding analytical an solution is not easy. Besides, numerical solutions, such as the Velocity Verlet [43] algorithm are found to obtain a particle's position after a certain time interval.

Periodic boundary calculations are applied to represent whole system properties in one simulation box, in a reasonable computation time.

#### **2.1.4. Minimization Methods**

For relaxation of the whole system before running MD simulations, a toolbox implemented to Materials Studio software is used. Discover Smart Minimizer module is used in order to proceed with minimization [29]. Smart minimizer combines several minimization methods and runs them respectively to result in an effective minimization procedure. It starts with steepest descent method and then it switches to conjugate gradient method and ends with Newton method. However, we used only steepest descent and conjugate gradient methods because Newton method requires extremely large computer storage due to computation and storage of second derivatives, and is recommended for systems consisting of a maximum of 200 atoms.

Steepest descent is a first order minimization algorithm that quickly reduces overall energy of the structure to lower values in a few steps. Method moves in the direction of the net force. As the gradient is very large in the initial structures, lower energy values are easily approached.

After steepest descent, an iterative algorithm, conjugate gradient method is used. Conjugate gradient method uses previous data to calculate later directions. It is being used for large systems where storing a second derivative matrix data are difficult. Since

it contains second derivative calculations, it is more time consuming than steepest descent, however, it is compensated by effective convergence. In our calculations, the Fletcher-Reeves algorithm is used [44].

### 2.1.5. COMPASS Force Field

COMPASS [35] is a condensed-phase optimized ab-initio force field. It enables accurate and simultaneous prediction of structural, conformational, vibrational and thermophysical properties for a broad range of molecules in isolation and in condensed phases including common organic molecules, inorganic small molecules and polymers. It has same functional forms with other forcefields such as CFF or PCFF [45], but they differ in parameterization in terms of interactions between various functional groups.

The functional forms of this forcefield are the same as CFF93 [46]:

$$\begin{aligned}
E_{Total} &= E_b + E_\theta + E_\phi + E_\chi + E_{bb'} + E_{b\theta} + E_{b\phi} + E_{\theta\theta'} + E_{\theta\theta'\phi} + E_{elec} + E_{LJ} \\
&= \sum_b \left[ K_2(b-b_0)^2 + K_3(b-b_0)^3 + K_4(b-b_0)^4 \right] \\
&+ \sum_\theta \left[ H_2(\theta-\theta_0)^2 + H_3(\theta-\theta_0)^3 + H_4(\theta-\theta_0)^4 \right] \\
&+ \sum_\phi \left[ V_1(1-\cos\phi) + V_2(1-\cos 2\phi) + V_3(1-\cos 3\phi) \right] + \sum_\chi K_\chi(\chi-\chi_0)^2 \\
&+ \sum_{b,b'} F_{b,b'}(b-b_0)(b'-b'_0) + \sum_{b,\phi} F_{b\theta}(b-b_0)(\theta-\theta_0) + \sum_{b,\phi} (b-b_0) \\
&\left[ F_{b,\phi}^{(1)}(1-\cos\phi) + F_{b,\phi}^{(2)}(1-2\cos\phi) + F_{b,\phi}^{(3)}(1-3\cos\phi) \right] \\
&+ \sum_{\theta,\theta'} F_{\theta,\theta'}(\theta-\theta_0)(\theta'-\theta'_0) + \sum_{\theta,\theta'\phi} F_{\theta,\theta'\phi}(\theta-\theta_0)(\theta'-\theta'_0)\cos\phi \\
&+ \sum_{i,j} \frac{q_i q_j}{\epsilon_0 r_{ij}} + \sum_{i,j} \epsilon_{ij} \left[ 2 \left( \frac{r_{ij}^0}{r_{ij}} \right)^9 - 3 \left( \frac{r_{ij}^0}{r_{ij}} \right)^6 \right]
\end{aligned} \tag{2.19}$$

This potential function can be investigated into two categories: valence terms including diagonal and off-diagonal cross couplings and nonbonded interaction terms.  $E_b$ ,  $E_\theta$ ,  $E_\phi$  and  $E_\chi$  represent bond, angle, torsion and out-of-plane angle coordinates, respectively. Also,  $E_{bb'}$ ,  $E_{b\theta}$ ,  $E_{b\phi}$ ,  $E_{\theta\theta'}$  and  $E_{\theta\theta'\phi}$  stand for cross-coupling terms, bond-bond  $E_{bb'}$ , bond-angle  $E_{b\theta}$ , and bond-torsion  $E_{b\phi}$  between internal coordinates which

helps to predict vibrational frequencies and structural variations associated with conformational changes.

## **2.2. Systems Studied**

### **2.2.1. Fluorinated Block Co-Oligomer Systems**

Block co-oligomer systems have of two or more repeat unit types with different chemical properties [47-50]. The self-assembly properties of block co-polymers originate from the chemical incompatibility between the blocks. They have a tendency to phase separate due to the long-range forces. The balance between repulsive and attractive forces on the macroscopic scale lead to ordered, complex mesoscopic morphologies by self-assembly. So, type, length or sequence of blocks play a crucial role on the final morphology obtained [50-54].

Within these groups of polymeric systems, fluorinated blocks have an important place that characterizes properties such as superhydrophobicity, high selectivity, bioinertness, low absorbance to UV light and solubility in supercritical carbon dioxide applications [55, 56]. It is predicted that fluorine containing block co-polymeric systems can be used in biomedical coatings or they can replace hazardous solvents in microlithography with supercritical carbon dioxide [13, 57].

#### **2.2.1.1. System Formation for Simulations**

In this work, poly (styrene-co-perfluoroalkylethylacrylate) (styrene-co-PFA) and poly (methylmethacrylate-co-perfluoroalkylethylacrylate) (methylmethacrylate-co-PFA) co-oligomers are selected as the systems of interest. In the experimental studies by Menciloglu group [27] concentration of PFA in styrene is 5 mole %, and solvent is chosen as tetrahydrofuran (THF). The same parameters and conditions are applied in the simulations as well. Concentration range of the co-oligomer inside solvent is varied between 10 and 100 % in order to observe full characteristics of the structures generated.

PFA co-polymer is initiated with ten units of styrene molecule  $-C_6H_5-CH=CH_2-$  (bead A), one repeat unit of solvophilic part of the PFA molecule  $-H_2C=(CH)-(C=O)-O-(CH_2)_2-$  (bead B) and seven repeat units of solvophobic part of the PFA molecule  $-CF_2-(CF_2)_5-CF_3-$  (bead D), respectively (Figure 2-1). So, the sequence of a co-oligomer is represented as;  $A_{10}B_1D_7$  for the coarse graining. The only difference in MMA-co-PFA co-oligomer is it starts with methylmethacrylate. Solvent molecule is represented by bead C.

Bead formation with respect to the molecules is shown in Figure 2-1.

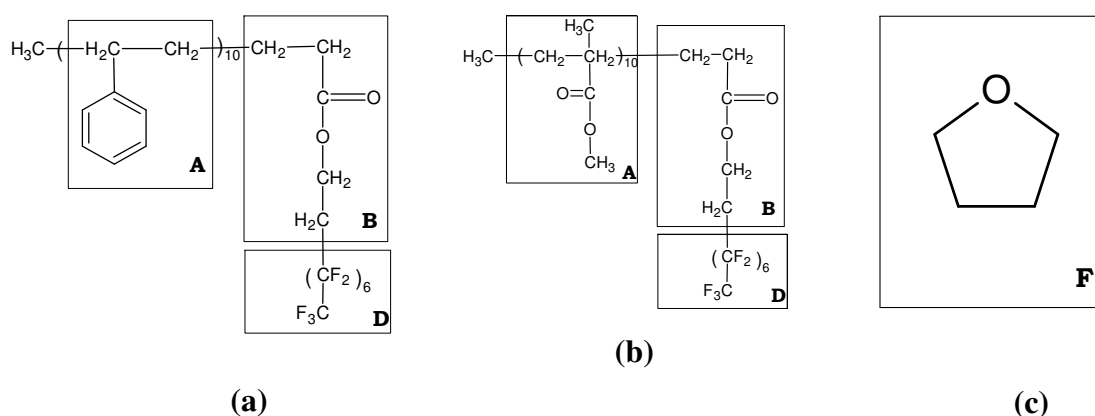


**Figure 2-1.** (a) Styrene-co-PFA and (b) Methylmethacrylate-co-PFA co-polymers (c) Tetrahydrofuran (THF) as solvent.

### 2.2.2. Surfactant Systems

It was previously discussed that it is of great importance to study self-assembly behavior of surfactant systems in order to design them. Apart from experimental techniques [58, 59] such as NMR, X-Ray, and EPR, computer simulation methods are being used to investigate self-assembly of surfactant.

In this study, oligomers are used that are organized by supercritical carbon dioxide, which is one of the most widely used for its low cost, low toxicity and easiness of recyclability. Compounds that have low cohesive energy such as, fluorocarbons,

fluoroethers [60-64], siloxanes [65] and polycarbonates [66] have a tendency to be easily solvated in surfactant because of their quadrupole and Lewis acidity characters. Besides, commercially available surfactants have very low CO<sub>2</sub> solubility, and cannot form stable micelles in it [67]. In order to overcome this problem, surfactants are modified with CO<sub>2</sub>-philic units [28, 60].

To investigate different side groups and oligomer lengths on the morphologies ABCBA type model surfactants have been designed. The model block co-oligomers used in this study is comprised of the CO<sub>2</sub>-phobic block having ethyl propionate and nine different types of ethylene monomers, flanked on either side by eight units of fluorinated CO<sub>2</sub>-philic blocks.

CO<sub>2</sub>-philic and fluorine containing segment of surfactant molecule -CF<sub>2</sub>CF<sub>3</sub>- is selected as A bead, ethyl propionate containing CO<sub>2</sub>-phobic block is selected as B bead, and for C bead CO<sub>2</sub>-phobic part in one of the nine types of ethylene monomers of the other surfactant is selected. CO<sub>2</sub> which is the solvent molecule is labeled as the D bead. Molecular structures of ABCBA type model surfactant is given in Figure 2-2 with nine types of R group in their CO<sub>2</sub>-phobic part.

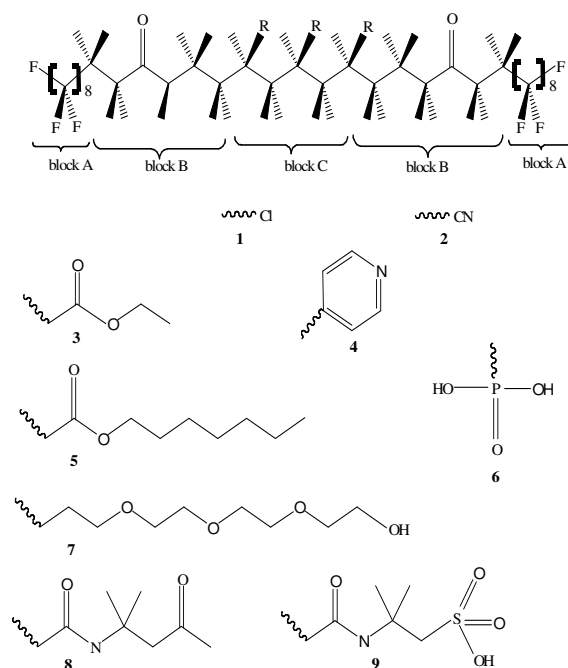


**Figure 2-2.** Molecular structures of ABCBA type model surfactant oligomer, with the nine different types of R groups in the CO<sub>2</sub>-phobic segment.

Sequence of the surfactant is represented as  $A_nB_1C_3B_1A_n$  where  $n$  is changed between 2-7.

### 2.3. Atomistic Detail Reverse Mapping Algorithm

Atomistic detail reverse mapping algorithm is based on fitting energy minimized templates that constitute the same atomic structure of the beads to be fitted. Coordinates of center of mass of the beads are known and centers of mass of the templates are calculated at the first step. Then, these templates are translated as their coordinates of the center of mass will be the same.

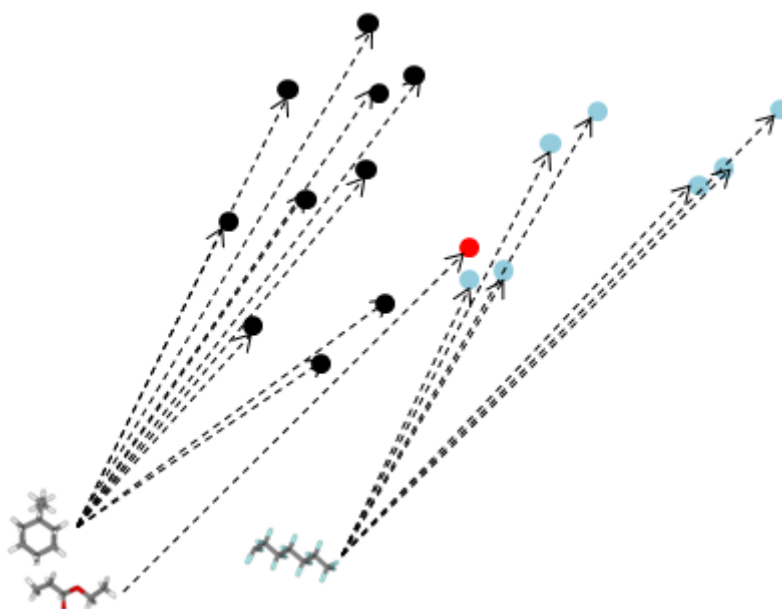


**Figure 2-3.** Center of masses of molecules are translated to coordinates of beads. The  $A_{10}B_1D_7$  system is shown schematically (see section 2.2.1.1) black, red and blue dots are styrene, hydrophobic part of PFA and fluorinated part of PFA, respectively.

For example, if a bead is constructed as  $-\text{CH}_2\text{OCH}_2\text{O}-$  then the template will be the bead itself. In this algorithm, templates need to be rotated around their centers of mass in order to satisfy the minimum cumulative distance between the first atom (C atom) of the later template and the last atom (O atom) of the former template. Distances between each two O-C atoms are shown as a vector,  $\vec{r}_{xyz}$ .

As the first step, angles between these templates are calculated in order to be used in the 3-D rotation matrix. Assumption of each angle between templates is a combination of angles for  $x$ -,  $y$ - and  $z$ - axes is made. So, as mentioned before, three angles are used in the 3-D rotation matrix to satisfy a unique rotation. The idea behind constructing rotation angles is to take projections of these  $\vec{r}_{xyz}$  vectors onto three planes  $x$ - $y$ ,  $y$ - $z$  and  $x$ - $z$  and to calculate angles between  $\vec{r}_{xyz}$  and each of these planes with triangles constructed with these projections. Projections of these vectors onto all of the axes are shown in Figure 2-4.

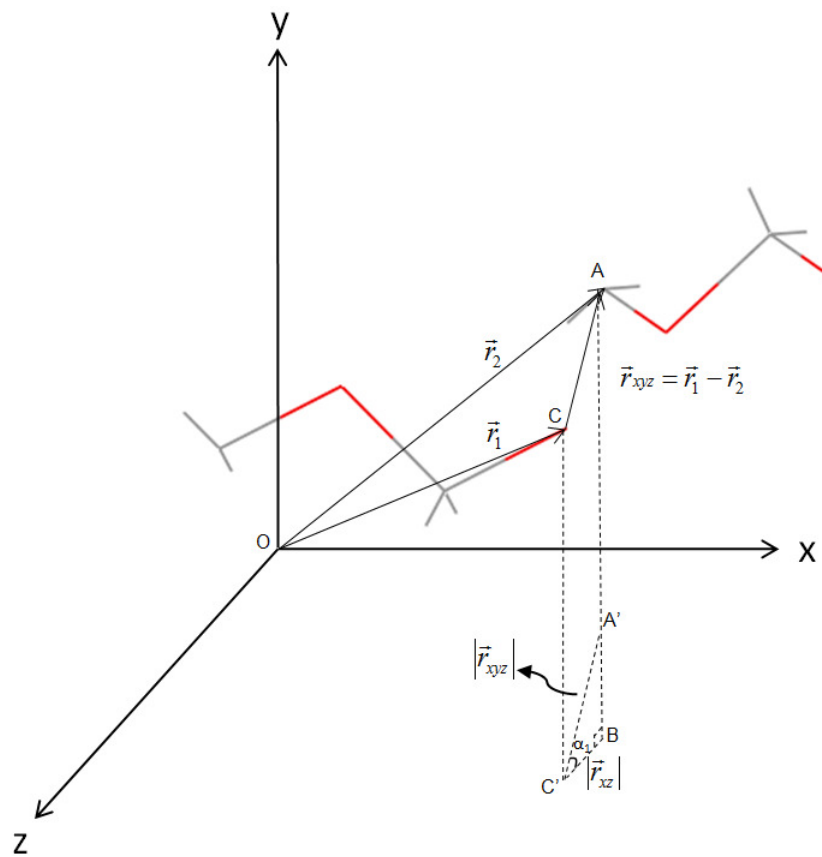


**Figure 2-4.** Projection onto the  $x$ - $z$  plane.

In Figure 2-4, projection onto  $x$ - $z$  plane is shown. A hypohetic right triangle is constructed by taking magnitudes of  $\vec{r}_{xyz}$ ,  $BC'$  and  $A'B$  vectors into consideration. Magnitude of  $\vec{r}_{xyz}$  vector is the hypotenuse of the  $A'BC'$  triangle,  $\alpha_1$  is  $A'C'B$  angle which is the angle between  $y$ -axis component and  $x$ - $z$  plane components of  $\vec{r}_{xyz}$  vector and  $BC'$  is projection of the  $\vec{r}_{xyz}$  vector onto  $x$ - $z$  plane. In other words,  $\alpha_1$  is angle of

deviation from the normal of  $x$ - $z$  plane. This angle can also be considered as rotation of  $y$ -axis component of  $\vec{r}_{xyz}$  vector. Projection of  $\vec{r}_{xyz}$  vector onto the  $x$ - $z$  plane is calculated by ignoring  $y$ -axis coordinates and only taking the difference of  $x$ - and  $z$ -coordinate values. Simply,  $|\vec{r}_{xz}|$  is calculated by using:

$$|\vec{r}_{xz}| = [(\vec{r}_{1x} - \vec{r}_{2x})^2 + (\vec{r}_{1z} - \vec{r}_{2z})^2]^{0.5} \quad (2.20)$$

Remaining steps for finding the angle are straightforward. Pythagoras Theorem is used in order to find the A'B distance and tangent value of the triangle is calculated by dividing A'B to BC' which gives ratio of sine to cosine of A'C'B angle. Hence, by taking the inverse of the tangent value, the angle is easily calculated.

In order to decide on the sign of angle, decrease or increase in the slope is considered. Negative slope means a negative angle value and vice versa. If coordinates of C atom of the latter template (i.e. point A) has a lower second axis value (for example  $y$ -axis value in  $x$ - $y$  plane) than the coordinates of O atom of the former template, the slope is given a negative value. Angles of rotation around  $x$ - and  $z$ -axes are calculated in the same way as angle of rotation around  $y$ -axis is calculated.

After calculating rotation angles for  $x$ -,  $y$ - and  $z$ - directions, they are implemented into the 3-D elementary rotation matrix. Rotation matrix is a transformation matrix that rotates a point clockwise. 3-D elementary rotation matrix is shown below.

$$M = \begin{bmatrix} \cos \alpha_1 \cos \alpha_2 & \cos \alpha_3 \sin \alpha_2 + \sin \alpha_3 \sin \alpha_1 \cos \alpha_2 & \sin \alpha_3 \sin \alpha_2 - \cos \alpha_3 \sin \alpha_1 \cos \alpha_2 \\ -\cos \alpha_1 \sin \alpha_2 & \cos \alpha_3 \cos \alpha_2 - \sin \alpha_3 \sin \alpha_1 \sin \alpha_2 & \sin \alpha_3 \cos \alpha_2 + \cos \alpha_3 \sin \alpha_1 \sin \alpha_2 \\ \sin \alpha_1 & -\sin \alpha_3 \cos \alpha_1 & \cos \alpha_3 \cos \alpha_1 \end{bmatrix} \quad (2.21)$$

where  $\alpha_1$ ,  $\alpha_2$  and  $\alpha_3$  are angles around  $y$ -,  $x$ -,  $z$ - axes, respectively.

Finally, final coordinates of the system is obtained by multiplying M with initial coordinates of system to be rotated.

$$A' = M \times A \quad (2.22)$$

Rotation matrix  $M$  is constructed by combining rotations in  $x$ -,  $y$ - and  $z$ - axes by taking the respective angles into consideration:

$$M = M_{\alpha_2} M_{\alpha_1} M_{\alpha_3} \quad (2.23)$$

where rotation matrices for three axes have the form:

$$M_{\alpha_2} = \begin{bmatrix} \cos \alpha_2 & \sin \alpha_2 & 0 \\ -\sin \alpha_2 & \cos \alpha_2 & 0 \\ 0 & 0 & 1 \end{bmatrix} \quad M_{\alpha_1} = \begin{bmatrix} \cos \alpha_1 & 0 & -\sin \alpha_1 \\ 0 & 1 & 0 \\ \sin \alpha_1 & 0 & \cos \alpha_1 \end{bmatrix} \quad M_{\alpha_3} = \begin{bmatrix} 1 & 0 & 0 \\ 0 & \cos \alpha_3 & \sin \alpha_3 \\ 0 & -\sin \alpha_3 & \cos \alpha_3 \end{bmatrix} \quad (2.24)$$

This is an iterative procedure and the target is to minimize the sum of the magnitudes of  $\vec{r}_{xyz}$  vectors. So, it is put as a constraint into the loop of calculations. At every step, angles between mentioned planes and distance vectors change and iteration continue until minimum values are satisfied.

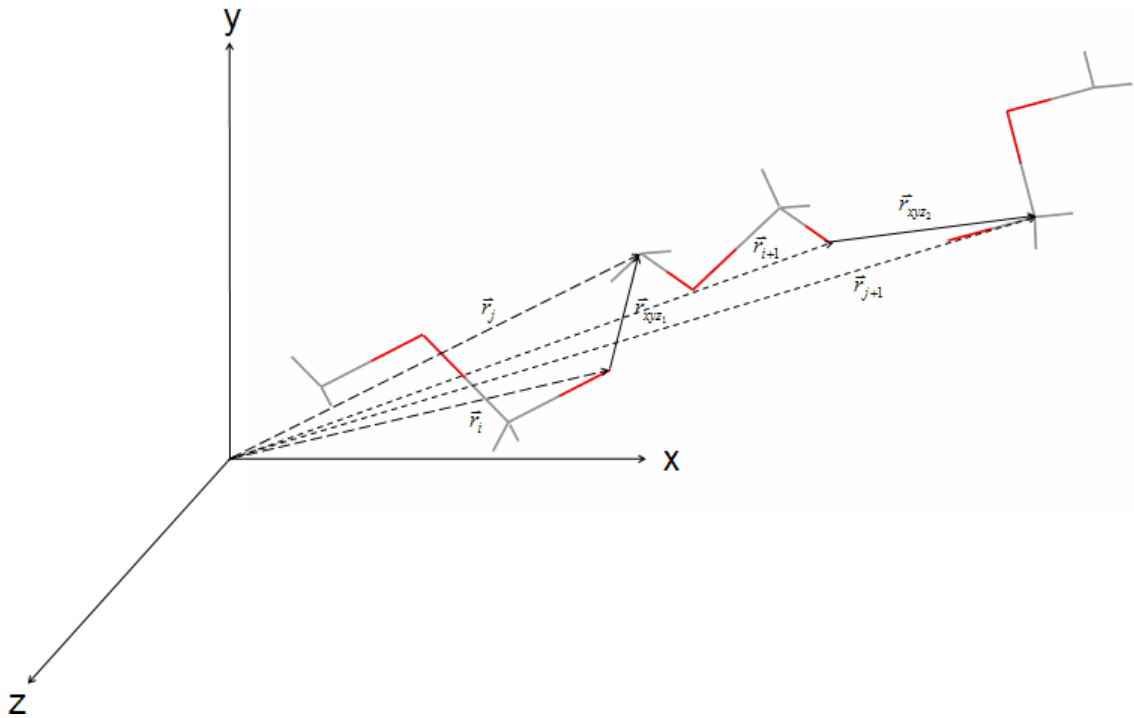


**Figure 2-5.** Distance vectors between consecutive templates.

Calculations of  $\vec{r}_{xyz}$  vectors are done at the beginning of each iteration. That is, after rotating a template, the distance to the later one is taken as equal to its value before rotation. Final positions of all templates are revised after each iteration is completed. Hence, these two steps are applied to the spherical system of styrene-co-PFA oligomer that is followed by an energy minimization step.

#### 2.4. Calculating the realistic length scales of the DPD systems

Since every data obtained as output from DPD simulation method is unitless, in order to match atomistic detail to DPD coordinates, we need to select a scale factor that enables matching DPD units to real length scales. In order to achieve that purpose, first volumes of each molecule corresponding to the beads are calculated.

**Table 2-1.** Amount and type of beads with corresponding molecular structures in one box.

<b>Bead Type</b>	<b>Molecule Name</b>	<b>Number of Beads in a Box</b>	<b>Volume of Each Molecule (<math>\text{\AA}^3</math>)</b>
A	Styrene	340	115.3
B	Linker	34	109.6
D	Fluorinated	238	226.4
F	THF	5400	79.7

The scaling factor calculation is based on the idea of volumes occupied by bead system and its corresponding molecular system should be proportional by this scaling factor. For example, there are approximately 6000 beads filling 10x10x10 volume in DPD units. If total real volume of corresponding volumes is calculated for the same system by multiplying number of each bead with volume of each molecule, then a total molecular volume of 527000  $\text{\AA}^3$  is obtained. Furthermore, it is known that packing factor for a crystal structure is around 70 %. So, if total volume is divided by this packing factor value, total approximate volume of the box is obtained as; 775000  $\text{\AA}^3$ . In addition, since total volume of the box is 1000 DPD unit cube, a DPD unit is found to be equivalent to 8.6  $\text{\AA}$ .

Since there are several assumptions in the calculation of the scaling factor, in order to check its consistency, RMSD values for a sample styrene-co-PFA chain between atomistic detail fitted structure and its energy minimized forms are calculated for different scaling factors around 8.6 Å. Minimum RMSD value shows how these two structures are similar in terms of length scales and with this RMSD, the actual mapping is satisfied.

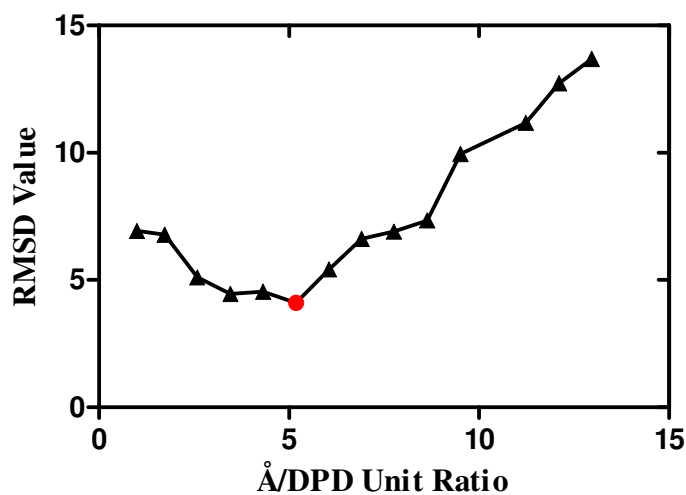


**Figure 2-6.** Scale factor of a DPD unit is determined by selecting minimum RMSD value of two conformations of a styrene-co-PFA chain (circle).

Hence, the minimum RMSD, the closest two structures, are found if scale factor is selected as 5.2 Å, that is decided as one DPD unit for further calculations.

### 3. RESULTS AND DISCUSSION

#### 3.1. DPD Simulations

##### 3.1.1. Fluorinated Co-Oligomer Systems

###### 3.1.1.1. Styrene-co-PFA System

DPD simulation results showed various morphologies of the block co-oligomer. Morphologies mostly comprised of micellar structures varying from spherical to cylindrical. Also, there is lamellar structure obtained with pure oligomer concentration. Box sizes are constructed as  $10 \times 10 \times 10 r_c^3$  for this system where  $r_c$  is the cut-off radius. The interaction parameters calculated via equation 2.7 are listed in Table 3-1.

**Table 3-1.** Interaction parameters ( $a_{ij}$ ) of fluorinated Styrene-co-PFA system (in  $k_B T$  units).

$a_{ij}$	A	B	D	F
A	25.0			
B	26.0	25.0		
D	38.4	48.7	25.0	
F	25.7	25.0	36.3	25.0

When we examine the DPD interaction parameters, we find that there are repulsive interactions between A-D and B-D beads due to the difference in their  $a_{ij}$  values. However, neutral interaction is observed between A and B beads, explained by low values of DPD interaction parameters. There is also repulsive interaction between D and F bead which is fluorinated part of PFA molecule and solvent bead, respectively. Hence, this type of interactions cause micro-phase separation in this block-copolymer

system due to covalent bonds. In figure 3-1 we display the final morphologies obtained for these systems.

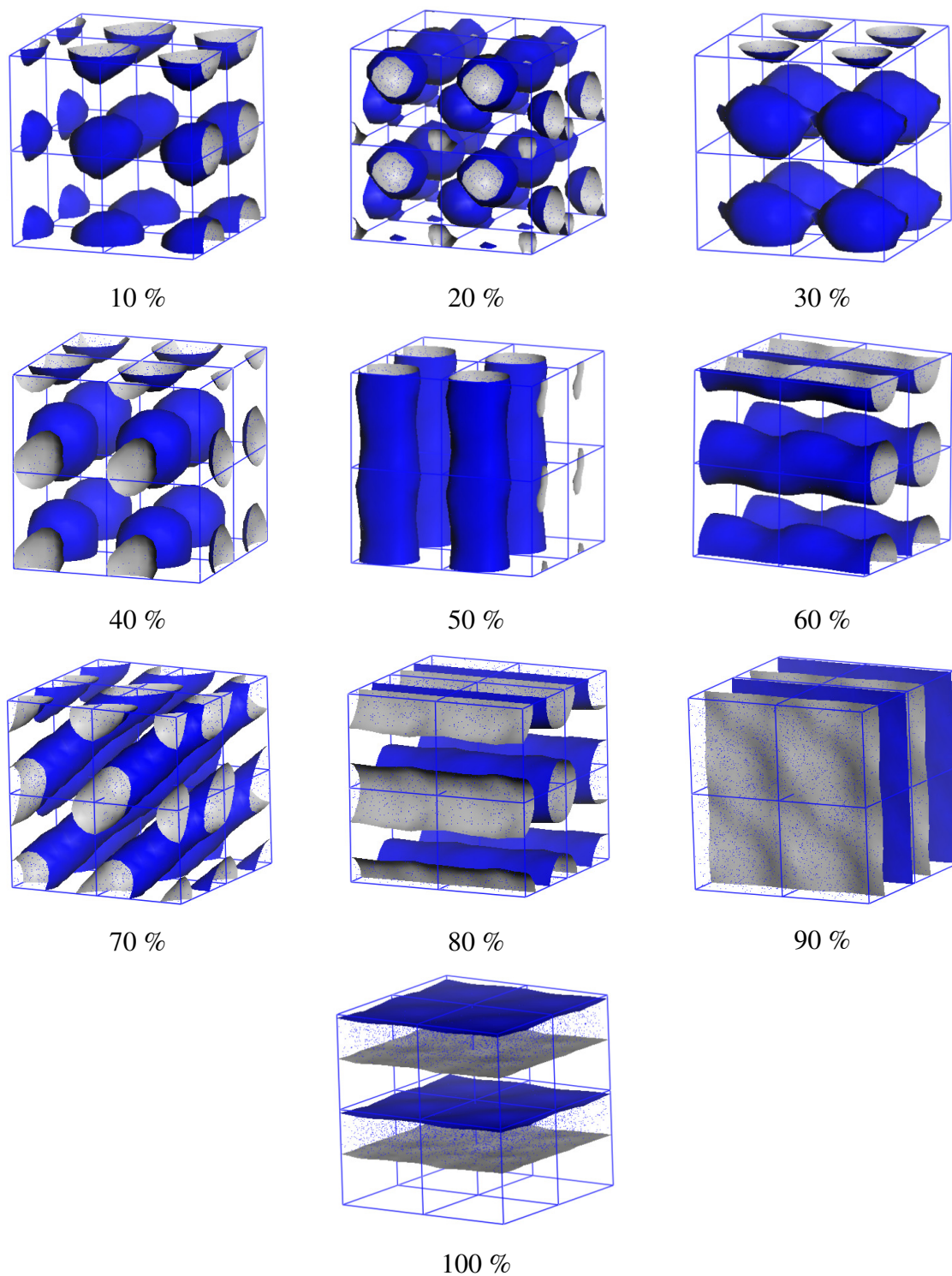


**Figure 3-1.** Mesoscopic morphologies obtained due to various molar compositions of Styrene-co-PFA oligomers in THF solvent.

Morphologies have been shown in terms of one bead type, D bead, and micro-phase separation can be seen clearly in the box. We can see that THF is a good solvent for styrene molecule due to closer values of interaction parameters. On the other hand, fluorinated part of PFA molecule and THF has tendency to phase separate because of the significant difference of  $a_{ij}$  values. These types of repulsive interactions are observed better in higher solvent concentrations until 50 %. If we decrease concentration of solvent in the box, structure switches to cylindrical micellar at 80 % co-oligomer and reached to lamellar structure at 90 % solute concentration.

### 3.1.1.2. MMA-co-PFA System

As a second system of block co-oligomer, MMA-co-PFA is studied in the same solvent, THF. PFA has a concentration of 5 % in the oligomer chain as in the experimental studies [27]. Corresponding morphologies between 10 % and 100 % are obtained. System is constructed in a similar way to the styrene containing oligomer. DPD interaction parameters calculated from equation 2.7 are listed in Table 3-2.

**Table 3-2.** Interaction parameters ( $a_{ij}$ ) of fluorinated MMA-co-PFA system (in  $kT$  units).

$a_{ij}$	<b>A</b>	<b>B</b>	<b>D</b>	<b>F</b>
<b>A</b>	25.0			
<b>B</b>	25.0	25.0		
<b>D</b>	49.5	48.7	25.0	
<b>F</b>	25.0	25.0	36.3	25.0

Before starting the simulations, interaction parameters are used to make predictions about the resulting morphologies. The values of parameters are similar as in the styrene system. There are repulsive interactions between A-D, B-D and D-F beads and attractive interactions between A, B and solvent bead F. This case is very similar to the styrene co-oligomer system case except that A-D repulsions are much stronger here. So, we expect similar morphological behavior for this system; the calculated morphologies are shown in figure 3-2.

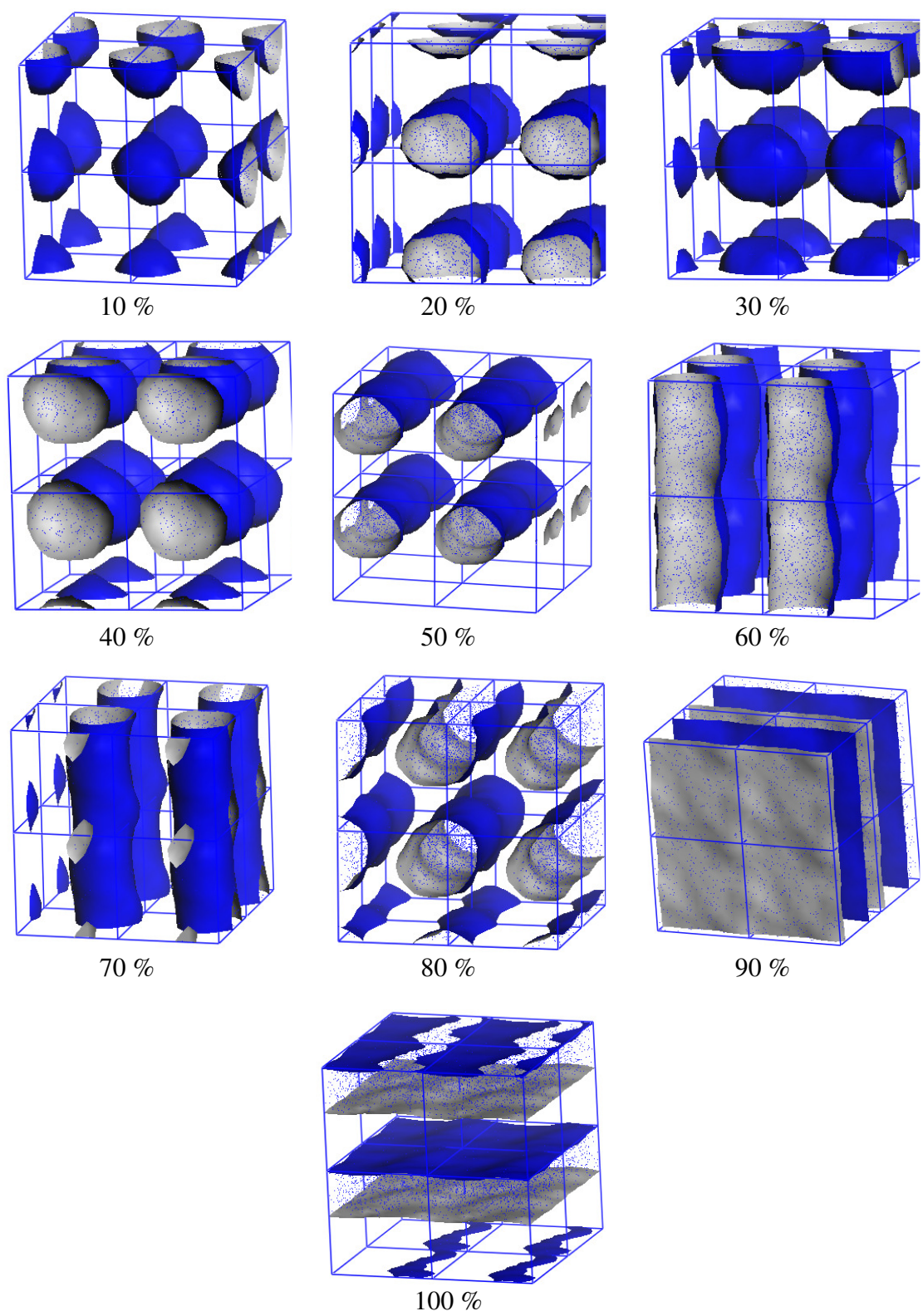


**Figure 3-2.** Mesoscopic morphologies obtained due to various molar compositions of MMA-co-PFA oligomers in THF solvent.

After investigation of the morphologies, we saw that similar micellar and lamellar formation has occurred in the simulation box. There are spherical micelles obtained until 40 % oligomer concentration but after that there is a sharp change of morphology to cylindrical micellar type after 50 % until 80 %. After that, lamellar morphology has been obtained at the very low concentrations of solvent, i.e. 90 %, that remains in its absence.

In summary, there is little morphological difference between styrene-co-PFA and MMA-co-PFA systems due to their very close values of interaction parameters. They represent the same characteristic according to concentration change. Although, interaction parameter value of A bead between D bead differs, it does not affect the morphology at the phase separation level.

### **3.2. Quantum Mechanical Calculations**

Quantum mechanical calculations are done to search for interactions that control structures of the fluorinated oligomers styrene-co-PFA and MMA-co-PFA in terms of attractive and repulsive interactions and electronic structures of molecules. For this purpose, local hardness values are calculated.

#### **3.2.1. Styrene-co-PFA Oligomer System**

For styrene containing fluorinated oligomer system, solubility parameters [29, 35] with local hardness values are given in the Table 3-3.

**Table 3-3.** Chemical reactivity values calculated for ring center on MP2/6-31G(d) level and solubility parameters for Styrene-co-PFA oligomer system.

	Solubility Parameters (cal/cm <sup>3</sup> ) <sup>1/2</sup>	Local hardness (a.u.)
Styrene (A)	7.9935	0.0516
Linker (B)	9.3315	0.0881
Flourinated (D)	3.9228	0.0397
Solvent (F)	9.3123	0.0809

Repulsive interactions between D and F beads are explained because of the difference in their local hardness values, and they are consistent with solubility parameters. At the same time, closer values of local hardness show attractive forces between B and F bead and this attraction is also confirmed with solubility parameter values.

In addition,  $\pi$ - $\pi$  interaction is observed in neighboring styrene molecules. AIM theory is used to calculate interaction energies corresponding to the bond critical points between styrene molecules on the same chain and on different chains by using electron density topology. Interaction energy values are calculated as 3.5 kcal/mol for styrene on the same chain and decline to 1.5-2.0 kcal/mol for styrene molecules on different chains. Calculations are done in the absence of solvent and collapsing of styrene molecules in this medium explains micellar structures obtained by DPD simulations. On the other hand, B and D beads do not have this kind of interaction and they show a wide dispersion in the simulation box. Hence, AIM calculations are also useful for capturing different properties of the system as the chemical reactivity calculations in order to explain morphological behavior of systems. Moreover, these quantum scale interactions are observed to be valid also at the meso-scale defined by interaction parameters. Besides, interaction parameters are obtained by MD simulations which are on a different length scale between quantum and meso-. However, note that MD force fields are parameterized at the QM level. Therefore, there is already a link between solubility parameters and QM induced reactivity indices.

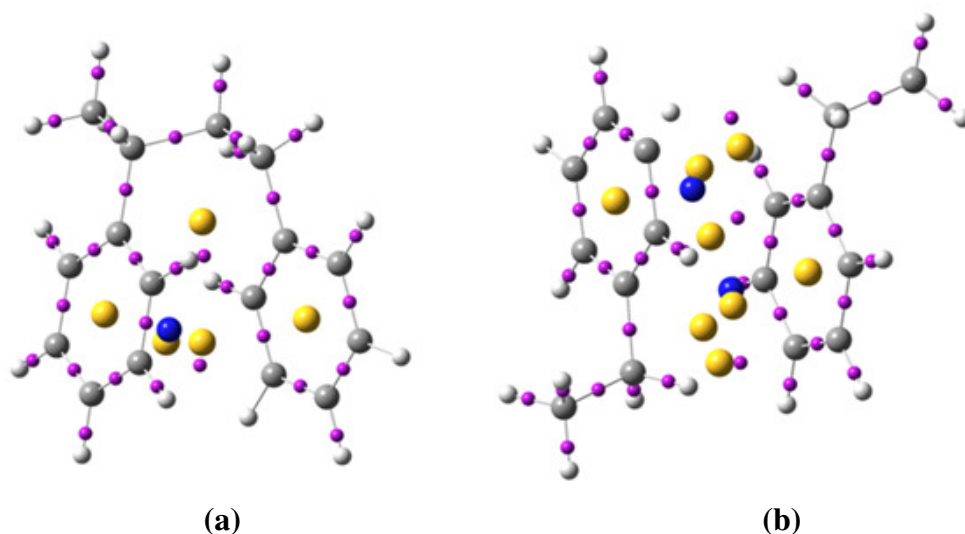


**Figure 3-3.** Interaction energy of styrene **(a)** on the same chain is 3.5 kcal/mol and **(b)** on different chains is 1.5-2.0 kcal/mol. Yellow, purple and blue dots show ring, bond and cage critical points, respectively.

### 3.2.2. MMA-co-PFA Oligomer System

Chemical reactivities in terms of local hardness values and AIM calculations are done in order to understand interactions at a different length scale for this oligomer system also. Same relationship as in styrene containing fluorinated oligomer case is obtained for this system. There are two local hardness values calculated for every bead. The reason behind this is to measure Molecular Electrostatic Potential (MEP) values 1.7 Å distant from two different points of molecule. For example, two values are calculated for C-O and C=O bonds of A bead.

We can see the difference in local hardness values of A, B, F beads with D bead that is related to the micro-phase separation in meso-scale. Phase separation can be investigated separately for D and F beads. Hence, chemical reactivity values in quantum scale and solubility parameter values in nanoscale together with DPD simulation results in meso-scale represent consistent results in all these length scales.

**Table 3-4.** Chemical reactivity values calculated on MP2/6-31G(d) level and solubility parameters for MMA-co-PFA oligomer system.

	Solubility Parameters (cal/cm <sup>3</sup> ) <sup>1/2</sup>	Local Hardness (au <sup>3</sup> )
MMA (A)	9.4202	0.0516 (C-O) 0.0458 (C=O)
Linker (B)	9.3315	0.0553 (C-O) 0.0436 (C=O)
Flourinated (D)	3.9229	0.0327 (Mid-chain) 0.0282 (End-chain)
Solvent (F)	9.3123	0.0539 (C-O)

### 3.3. Surfactant System

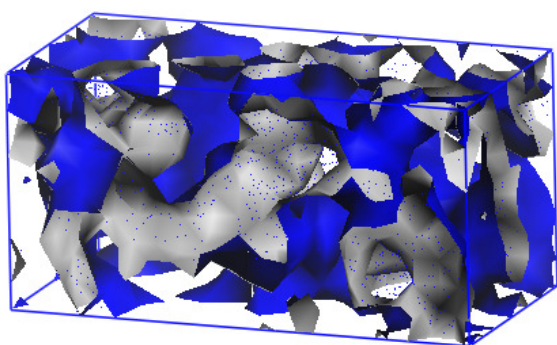
For this surfactant system, oligomers with nine side groups were studied. DPD interaction parameters for all of the systems are computed and found that the interactions between the variable center groups (C beads) and the linker (B beads) are uniform in value across different types. On the other hand, interactions between C bead with A and D beads show a wide range of interaction type. For example, oligomers 1 and 2 show nearly neutral interaction, however, oligomer 7 displays a dominantly repulsive interaction.

**Table 3-5.** Interaction parameters ( $a_{ij}$ ) of the compounds 1-9 (in  $kT$  units); also listed are the bead molar volumes.\*

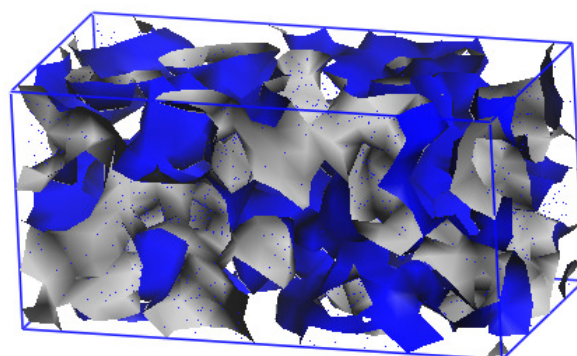
Compound	$a_{AC}$	$a_{BC}$	$a_{CD}$	$V_m$	<i>molar mass</i>
1	26.9	26.2	28.5	73	65
2	26.3	26.8	27.9	71	55
3	33.6	25.1	37.1	131	116
4	30.7	25.1	33.8	115	107
5	34.3	25.0	40.0	214	186
6	31.7	25.0	34.4	96	110
7	42.5	26.0	50.1	22	227
8	37.9	25.3	43.8	197	185
9	32.2	25.1	37.0	185	223

\*The following parameters are the same in all compounds:  $a_{AB} = 32.3$ ,  $a_{AD} = 25.5$ ,  $a_{BD} = 35.7$ ;  $V_m = 84, 125, 44$  for beads **A**, **B** and **D**, respectively; molar mass of these units are 102, 56, 44, respectively.

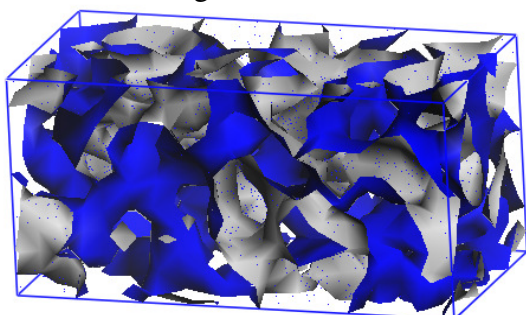
Each of the compounds were studied at specific concentrations in order to observe to form any micellar or lamellar structures. Oligomers 1-9 are simulated with two concentration values; 40 % and 80 % at 120 000 DPD steps. These oligomeric systems clustered into two groups according to their phase behavior, I (3, 5, 7-9) and II (1, 2, 4, 6). For group II, stable micellar structures are not observed. However, for oligomer 7, the most stable spherical and cylindrical micelles are seen at 40 and 80 %, respectively. The resulting morphologies are shown in figure 3-4.



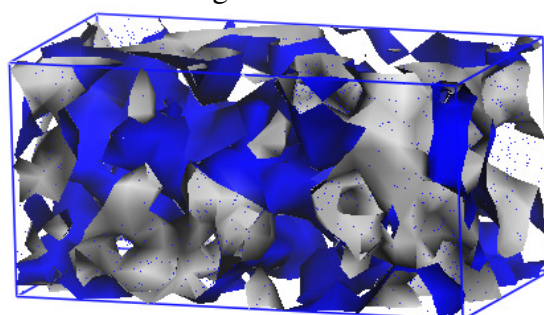
Oligomer 1-40 %



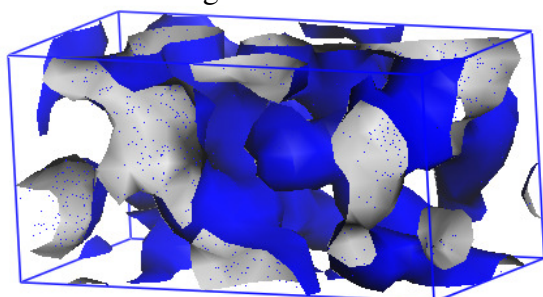
Oligomer 1-80 %



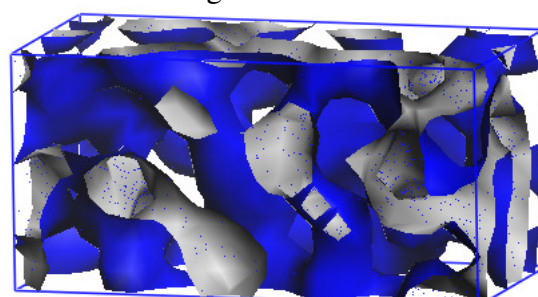
Oligomer 2-40 %



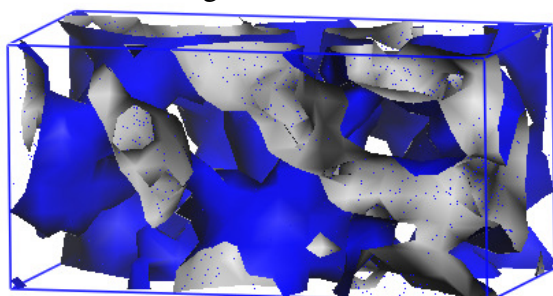
Oligomer 2-80 %



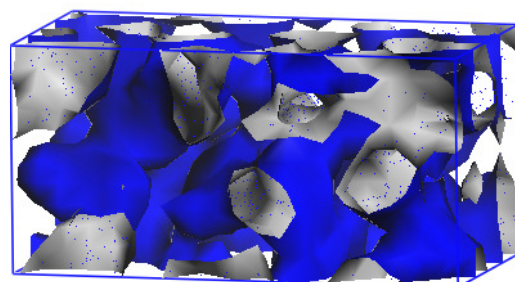
Oligomer 3-40 %



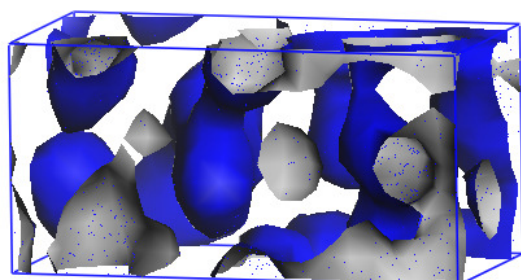
Oligomer 3-80 %



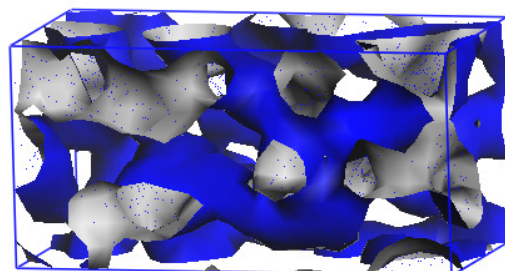
Oligomer 4-40 %



Oligomer 4-80 %



Oligomer 5-40 %



Oligomer 5-80 %

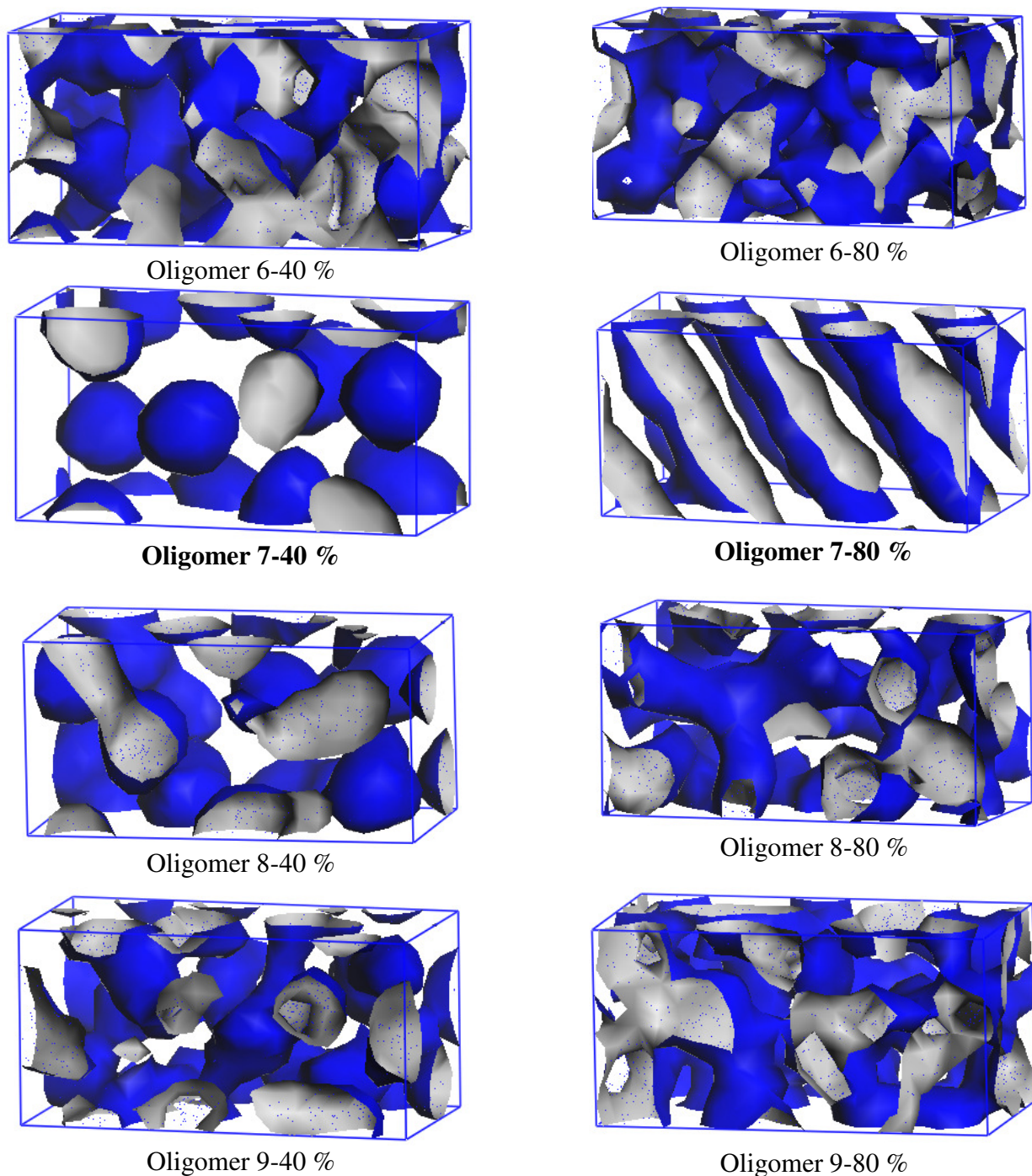


**Figure 3-4.** Morphologies obtained with respect to different type of side chains.

All of the snapshots with respect to concentrations of all oligomers are taken for bead type C because it contains the groups that form the core of the micelles. So, interaction parameters related to C gain more importance than other beads in obtaining morphological behavior of the system. Moreover, if we look at  $a_{ij}$  values of all oligomer systems, we can see that the values reached their highest for oligomer 7. Since these values characterize micro-phase separation of the system, it is logical to obtain good micellar structures for oligomer 7.

Spherical micellar structures are mainly the result of CO<sub>2</sub>-phobic interactions of the C bead. In this type of interaction, C bead is buried inside and fluorinated parts are located outside in order to minimize interactions with CO<sub>2</sub>.

In addition to the previous studies of obtaining morphology, we also computed surface to volume ratios ( $S/V$ ) of oligomer 7 system for all concentrations simulated. The idea in calculating  $S/V$  ratios of individual micelles is to investigate relative contributions of energetic and entropic factors to micelle formation. We know that, for spheres surface area to volume ratio is  $3/r$  and for cylindrical the value is  $2/r$  with average radius of  $r$ . We have used image processing algorithms to compute the radii of micelles whose images are captured during simulations. For image processing, MATLAB Image Processing Toolbox is used [68].

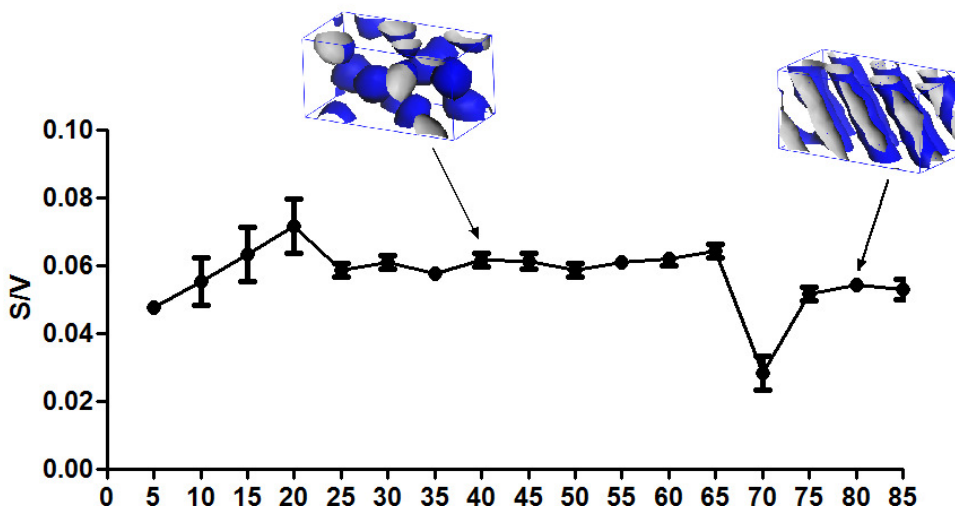


**Figure 3-5.** Surface area-volume ratios ( $S/V$ ) of micelles changing with respect to volume concentration of the oligomer.

When we look at the morphologies, first spherical micellar structures are obtained at 25 % and cylindrical structures are observed at 75 % oligomer concentration. In  $S/V$  versus oligomer concentration plot, there is a sharp decrease in the graph when we observe spherical micellar formation. Furthermore, phase change to cylindrical micelle takes place at 70 % concentration where  $S/V$  ratio is also decreased. Hence, spherical micelles have more ability in formation than cylindrical micelles due to their larger surface area to volume ratio.

We have studied the effect of concentration on the microstructure of the stable oligomer **7**, by varying the volume fraction from 5 to 100 %. The radial distribution functions,  $g(r)$ , of beads in the system are displayed in Figure 3-6. We find that the overall local structure in the system does not change with the oligomer concentration and the radial distribution function values of beads in these coordination shells are also the same. However, the identity of the beads in the local regions differs: The distribution of beads from the adjacent chains and the solvent decreases with increasing oligomer concentration (Figure 3-6b). Locally, they are replaced by beads residing on the same chain (Figure 3-6c). This change results in an overall decrease in the pressure of the systems (inset to figure 3-6a). The intramolecular interactions are always energetically less costly than intermolecular ones in the currently studied systems. Thus, favoring the intramolecular contacts over intermolecular ones, the virial,  $\frac{1}{3} \sum_{i=1}^N r_i \cdot f_i$  has a smaller contribution to the overall pressure as concentration is increased.

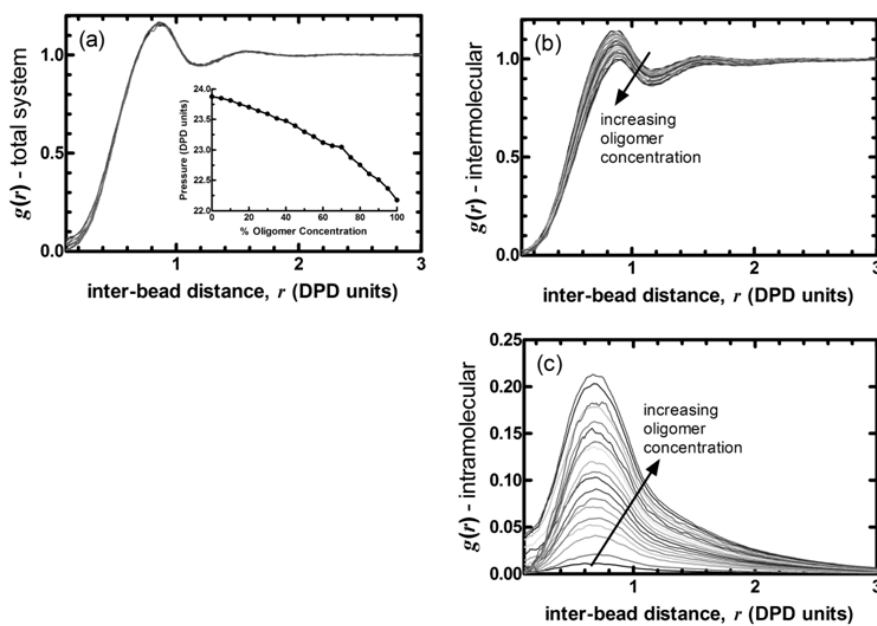


**Figure 3-6.** Variation in the radial distribution functions,  $g(r)$ , of beads in the system with oligomer concentration. (a) Total distribution of beads in the system does not change. The pressure, however, monotonically decreases with increasing concentration (inset). Intermolecular number density distribution of beads decreases with concentration (b), whereas intramolecular distribution increases.

After morphology is equilibrated, we have applied different shear stress ratios to the system in order to check for stable morphologies using slick boundary conditions [69]. We study only regular micellar structures corresponding to 40 % and 80 % for spherical and cylindrical structures, respectively at a shear rate of 0.001 and 0.01 for both of the systems. Moreover, shear stress is applied until 250 000 DPD steps in addition to equilibrated structure obtained with 120 000 steps. The resulting morphologies are shown in figure 3-7.

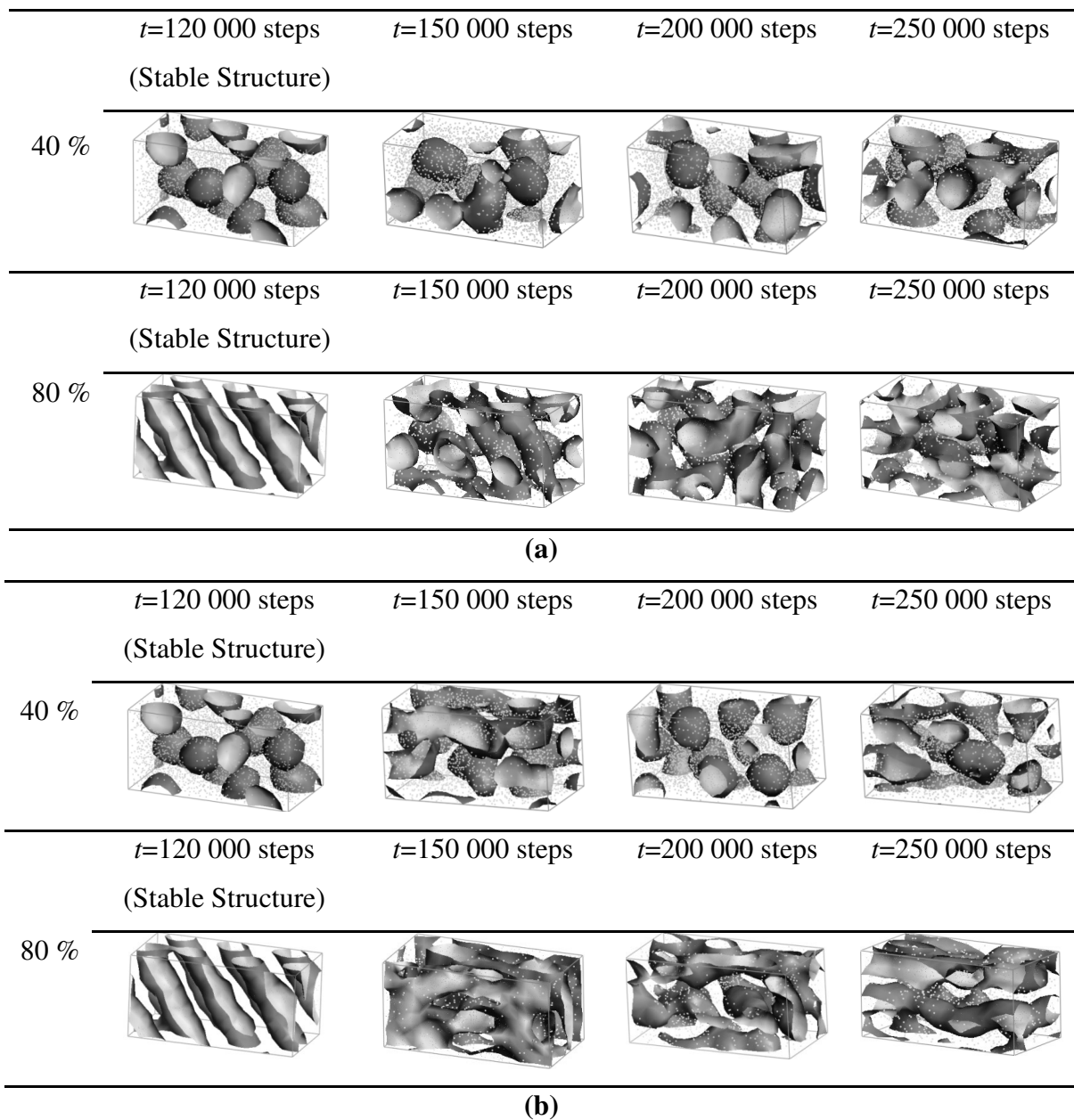


**Figure 3-7.** Morphologies obtained after applying (a) shear rate 0.001 and (b) shear rate 0.01.

Effect of higher value of shear stress (0.01) on spherical morphology is seen as a deviation from stable structure for all types of morphology oligomer system. However, shear stress rate of 0.001 does not affect morphologies for spherical micelle, but at the same shear stress rate, morphologies become irregular for cylindrical micelle at 80 %. Hence, the spherical micelles are more stable than the cylindrical ones, corroborating the result indicated by the  $S/V$  ratios that there is a larger energetic contribution in the former.

### **3.4. Reverse Mapping of Atomistic Detail**

A large effort in this work has gone into developing an algorithm based on fitting atomistic detail into structures obtained from meso-scale DPD simulations. Our algorithm contains differences from current reverse mapping algorithms in the literature. As a first step, we are not building molecules from a single atom; in contrast, we are using pre-built templates for fitting. Since algorithm contains minimization of distances between beads while rotation, it automatically optimizes structure to lower energy values. On the other hand, Tschop and co-workers [26] constructed the chain as their initial step, and then they tried to fit overall chain to original chain coordinates. However, we are building molecules into beads as a first step and satisfying optimum structure by rotating molecules in three dimensions without holding distances between molecules constant. This procedure increases degrees of freedom coming from rotation in three dimensions but searches many possible conformations to obtain lower energy values. Thus, the current methodology is similar to the local torsional deformations method used in the conformational search of molecules under restraint [70, 71]. In addition, since our algorithm is based on minimizing distances between molecules, we can study different types of molecules with different number of atoms of molecules constructing beads with little additional computational effort.

Center of masses of molecules corresponding to beads are fitted to DPD output coordinates which give positions of beads in the simulation box. Algorithm is applied to spherical system of micelles styrene-co-PFA which corresponds to 10 % concentration. 10 % concentration is the best structure that we have obtained during DPD simulations

in terms of spheres. It contains a single sphere in the box, so it is easier to visualize the overall structure after fitting.

For ease of representation, atomistic detail fitting algorithm applied to a single chain is represented in the figures. Figure 3-8 represent all of the steps; Translation, Rotation and Energy Minimization. In addition, RMSD (Root Mean Square Deviation) values are calculated in order to check the improvement in the algorithm. Hence, RMSD values are; 4.77 Å between translated and rotated, 3.58 Å between rotated and energy minimized structures. The RMSD value between translated and energy minimized structures and obtained as 5.21 Å.

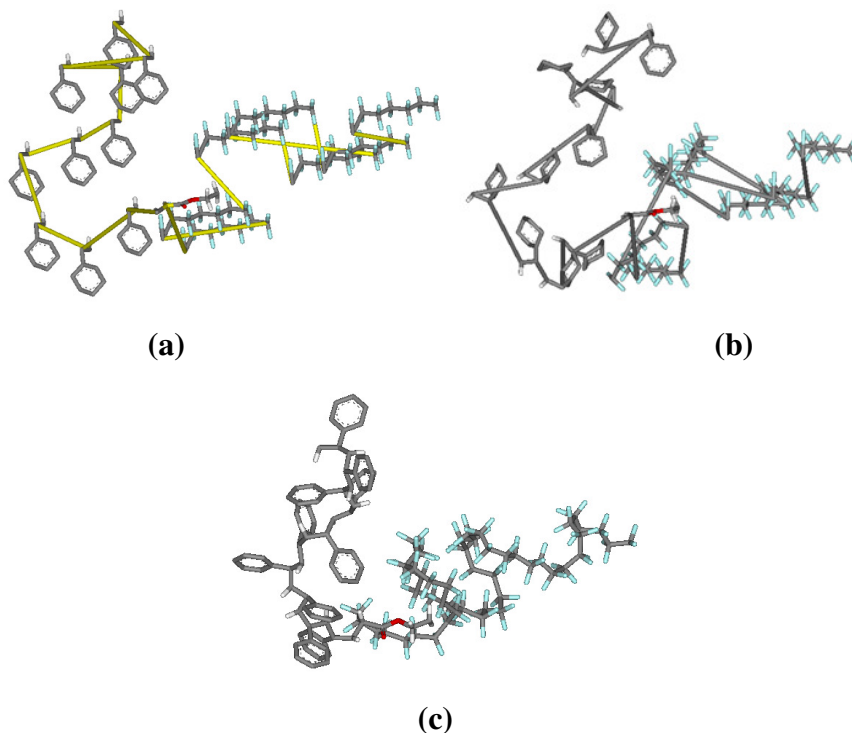


**Figure 3-8.** Atomistic detailed single Styrene-co-PFA oligomer chain structures obtained after (a) Translation, (b) Rotation and (c) Energy minimized.

Furthermore, algorithm is utilized as fitting energy minimized structures to the whole spherical morphology at the same time. Every single chain contains 18 beads and a sphere consists of A, B and D beads. There are 34 chains forming one sphere, leading to, 612 beads that are to be reverse mapped.

Since, there are 250 atoms in a single chain consisting of C, O, F and H atoms, there will be 8500 atoms after atomistic detail fitting algorithm is applied. The crucial

idea while fitting the atoms is that, algorithm need to prevent overlapping of the atoms. So, this is done by satisfying a certain criteria of controlling final positions of atoms after each molecule is fitted. Hence, overall system of atomistic detailed structures is reached.

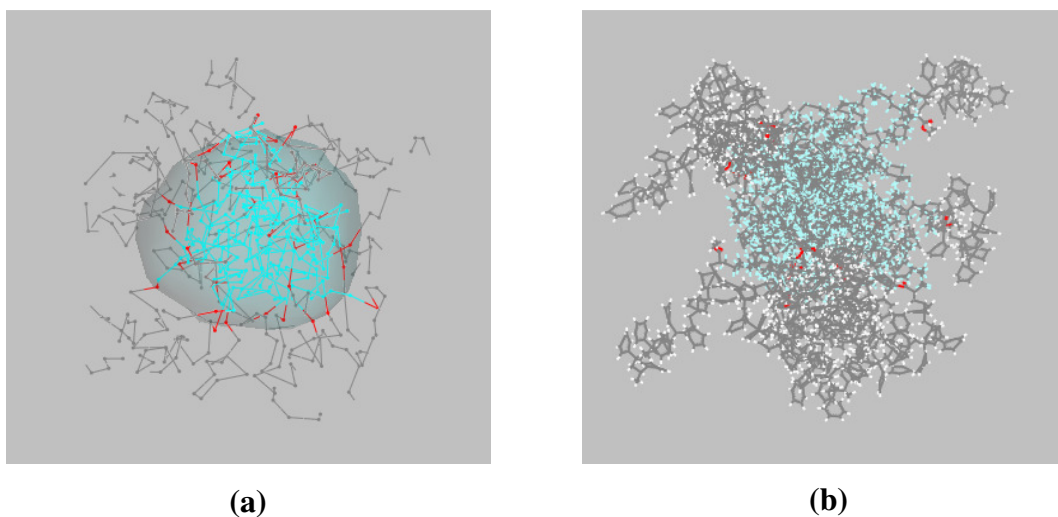


**Figure 3-9.** Spherical morphology of 10 % styrene-co-PFA oligomer system (a) consisting of beads, (b) after atomistic detail is reverse mapped.

After fitting procedure is applied, in order to study dynamics of the system, atomistic detailed structure is energy minimized up to 250 000 steps consisting of steepest descent and conjugate gradient, whole system is soaked into a periodic water box of 42 000 atoms.

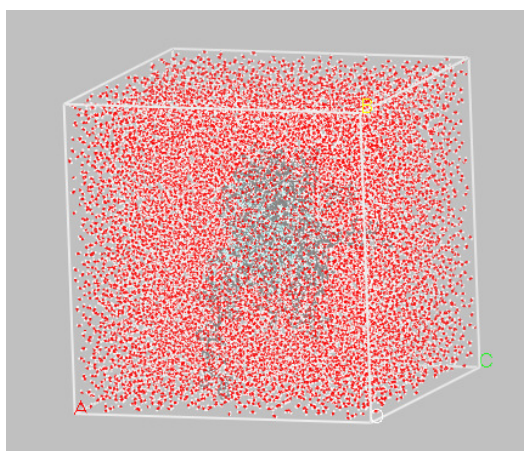


**Figure 3-10.** Atomistic detail reverse mapped styrene-co-PFA oligomer soaked into water box.

Since styrene-co-PFA polymer is known to construct superhydrophobic surfaces, its dynamics inside water is crucial to investigate. Although, there are proposed theories that search its interaction with water, they do not directly take atomistic scale details into account. So, running MD simulations in a water box will provide a better understanding of the dynamics at the native state.

#### 4. CONCLUSIONS AND RECOMMENDATIONS FOR FUTURE STUDIES

Self-assembly behavior of materials is becoming a widely studied area. Designing or developing brand new materials require a correct understanding of the structure on different length scales. Thus, studying materials from nano to meso-scale leads to predict structural behavior and properties of materials on macro-scale. Hence, inter-relating the results from techniques that operate on different length and time scales gains importance.

In this study, various co-oligomer systems are studied at different length scales to observe the relationship between them. Two types of co-oligomer systems are used: Fluorinated hydrophobic and CO<sub>2</sub>-phobic surfactant systems. Both of the systems contain fluorinated segments but as mentioned, they have different structural properties affecting their application areas.

First of all, fluorinated co-oligomer systems, Styrene-co-PFA, and Methylmethacrylate-co-PFA, are studied at the meso-scale to derive their three dimensional morphologies. Spherical and cylindrical micellar structures and lamellar morphologies are obtained with increasing oligomer. On the other hand, DPD simulation procedure is also applied to a surfactant system, again leading to spherical and cylindrical morphologies as concentration of solvent is decreased. For the systems under study, THF and CO<sub>2</sub> are used as solvent for fluorinated and surfactant system, respectively.

Secondly, quantum mechanical calculations are applied to Styrene-co-PFA and MMA-co-PFA system to better understand the interactions leading to these morphologies. The significant part of this step is to utilize knowledge from a much shorter length scale. Quantum level calculations are applied on both of the systems in terms of chemical reactivity values (local hardness) and AIM theory (interaction energies between molecules). It is observed that AIM calculations are more effective and explains micelle formation better than chemical reactivity calculations because it is observed that styrene molecules are found to be collapsing on each other in the absence

of solvent in the medium. So, this explains micelle formation while we increase solvent amount in the simulation box. On the other hand, MD simulations are applied to both of the systems and solubility parameters between molecules are derived. This is on an intermediate length scale, leading to consistent results with both the shorter and longer scales. That means, solubility parameters, which defines micro-phase separation and chemical reactivity values, that shows like-dislike behavior of molecules display the same characteristic for each of the systems. Hence, sphere and cylinder formation maybe predicted from quantum level calculations.

Surfactant system is studied on meso-scale in terms of behaviors of spherical and cylindrical micelles. Surface-to-volume ( $S/V$ ) ratios of systems for regular micellar structures, 40 % and 80 % are chosen.  $S/V$  show relative energetic and entropic contributions that derive the system to micelle formation. It is shown that, spherical micelles have higher  $S/V$  values than cylindrical micelles. And also, since micro-phase separation occurs, fluctuations in the  $S/V$  vs. concentration plot is expected. Hence, after calculating  $S/V$ , phase change due to different kind of micelle formation is observed clearly. In addition, internal pressure values are obtained from DPD output and plotted against concentration and it is seen a decline in internal pressure of the system while decreasing solvent concentration. Furthermore, shear stress is applied to equilibrated morphologies in order to test their stability. Two different shear stress rates are used and deviation from stable structures is observed for cylindrical structures for every shear stress value. On the other hand, spherical micellar structures are found to be more stable since the morphology is not affected from lower shear stress value. But, when shear stress rate is increased for spherical micelle, its morphology also deviates from that of the equilibrated structure.

Finally, fluorinated superhydrophobic spherical micelle is mapped to the atomic-scale. The reason behind this is that; we do not have any experimental depository for synthetic polymer systems to run MD simulations in order to understand their behavior in the medium of target. However, since DPD is a coarse-grained meso-scale method, it allows fast prediction of “folded” morphologies of synthetic self-assembly systems. Atomistic detail reverse mapping algorithm is applied in order to predict the locations of atoms in the final structures. A three step procedure is followed in the algorithm: First; molecules consisting of beads are translated onto coordinates obtained from DPD

output. Then, the molecules are rotated as the cumulative distance between them will be minimum and finally, overall system is energy minimized. The improvement in the algorithm is checked via comparing RMSD (Root Mean Square Deviation) results for three of the steps for a single chain. Then, it is satisfied that after the algorithm is applied, RMSD decreased with respect to the steps. Hence, final atomistic detailed structures are obtained for the aforementioned sphere.

For future work, in addition to this study, energy minimization of water box containing oligomer system will be performed and after minimization is completed, MD simulations will be applied to observe the dynamics of the system at the hydrophobic interface. Also, application of the reverse mapping algorithm to many systems will be performed to make a depository of coordinates that will be used as inputs for MD simulations.

## 5. REFERENCES

1. Taniguchi, N., *On the Basic Concept of 'NanoTechnology'*. Proc. of the ICPE, 1974. **2**: p. 18–23.
2. Coveney, P.V., *Self-organization and complexity: a new age for theory, computation and experiment*. Philosophical Transactions of the Royal Society of London Series a-Mathematical Physical and Engineering Sciences, 2003. **361**(1807): p. 1057-1079.
3. Uhlherr, A. and D.N. Theodorou, *Hierarchical simulation approach to structure and dynamics of polymers*. Current Opinion in Solid State & Materials Science, 1998. **3**(6): p. 544-551.
4. Leach, A.R., *Molecular Modeling, Principles and Applications*. 2001, England: Pearson Education.
5. Adler, B.J., Wainwright T. E. , J. Chem. Phys, 1957. **27**.
6. Atilgan, C., A.O. Aykut, and A.R. Atilgan, *How a vicinal layer of solvent modulates the dynamics of proteins*. Biophysical Journal, 2008. **94**(1): p. 79-89.
7. Berman, H.M., et al., *The Protein Data Bank*. Nucleic Acids Research, 2000. **28**(1): p. 235-242.
8. Srinivas, G., D.E. Discher, and M.L. Klein, *Self-assembly and properties of diblock copolymers by coarse-grain molecular dynamics*. Nature Materials, 2004. **3**(9): p. 638-644.
9. Ozen, A.S., U. Sen, and C. Atilgan, *Complete mapping of the morphologies of some linear and graft fluorinated co-oligomers in an aprotic solvent by dissipative particle dynamics*. Journal of Chemical Physics, 2006. **124**(6).
10. Groot, R.D. and P.B. Warren, *Dissipative particle dynamics: Bridging the gap between atomistic and mesoscopic simulation*. Journal of Chemical Physics, 1997. **107**(11): p. 4423-4435.
11. Flory, P.J., *Principles of polymer chemistry*. 1953, Ithaca: Cornell University Press.
12. Hoogerbrugge, P.J. and J.M.V.A. Koelman, *Simulating Microscopic Hydrodynamic Phenomena with Dissipative Particle Dynamics*. Europhysics Letters, 1992. **19**(3): p. 155-160.

13. Bilgin, N., C. Baysal, and Y.Z. Menciloglu, *Synthesis of fluorinated oligomers for supercritical carbon dioxide applications*. Journal of Polymer Science Part a-Polymer Chemistry, 2005. **43**(21): p. 5312-5322.
14. Guler, M.O. and S.I. Stupp, *A self-assembled nanofiber catalyst for ester hydrolysis*. Journal of the American Chemical Society, 2007. **129**(40).
15. Ulman, A., *Formation and structure of self-assembled monolayers*. Chemical Reviews, 1996. **96**(4): p. 1533-1554.
16. Thunemann, A.F., *Polyelectrolyte-surfactant complexes (synthesis, structure and materials aspects)*. Progress in Polymer Science, 2002. **27**(8): p. 1473-1572.
17. Israelachvili, J.N., *Intermolecular and Surface Forces*. 1997, London: Academic Press.
18. Parr, R.G.D., R. A.; Levy, M.; Palke, W. E., *Electronegativity: The density functional viewpoint*. The Journal of Chemical Physics, 1978. **68**.
19. Kohn, W., A.D. Becke, and R.G. Parr, *Density functional theory of electronic structure*. Journal of Physical Chemistry, 1996. **100**(31): p. 12974-12980.
20. Parr, R.G. and R.G. Pearson, *Absolute Hardness - Companion Parameter to Absolute Electronegativity*. Journal of the American Chemical Society, 1983. **105**(26): p. 7512-7516.
21. Pearson, R.G., *Journal of Chemical Education*, **1968**. **45**.
22. Sanderson, R.T., *An Interpretation of Bond Lengths and a Classification of Bonds*. Science, 1951. **114**.
23. Atilgan, C. and V. Aviyente, *Hybrid usage of computational tools in drug synthesis*. Current Computer-Aided Drug Design, 2007. **3**(2): p. 149-159.
24. Santangelo, G., et al., *From mesoscale back to atomistic models: A fast reverse-mapping procedure for vinyl polymer chains*. Journal of Physical Chemistry B, 2007. **111**(11): p. 2765-2773.
25. Chen, L.J., et al., *An automatic coarse-graining and fine-graining simulation method: Application on polyethylene*. Journal of Physical Chemistry B, 2006. **110**(47): p. 24093-24100.
26. Tschop, W., et al., *Simulation of polymer melts. II. From coarse-grained models back to atomistic description*. Acta Polymerica, 1998. **49**(2-3): p. 75-79.
27. Simsek, E., *Wettability Of Smooth And Rough Surfaces Of Perfluoroacrylate Copolymers in Materials Science and Engineering*. 2006, Sabanci University: Istanbul.

28. Kirmizialtin, S., Y.Z. Menciloglu, and C. Baysal, *New surfactants design for CO<sub>2</sub> applications: Molecular dynamics simulations of fluorocarbon-hydrocarbon oligomers*. Journal of Chemical Physics, 2003. **119**(9): p. 4953-4961.
29. Accelrys, I., *Materials Studio*. 2002: San Diego.
30. M. J. Frisch, G.W.T., H. B. Schlegel, G. E. Scuseria, M. A. Robb, J. R. Cheeseman, J. A. Montgomery, Jr., T. Vreven, K. N. Kudin, J. C. Burant, J. M. Millam, S. S. Iyengar, J. Tomasi, V. Barone, B. Mennucci, M. Cossi, G. Scalmani, N. Rega, G. A. Petersson, H. Nakatsuji, M. Hada, M. Ehara, K. Toyota, R. Fukuda, J. Hasegawa, M. Ishida, T. Nakajima, Y. Honda, O. Kitao, H. Nakai, M. Klene, X. Li, J. E. Knox, H. P. Hratchian, J. B. Cross, C. Adamo, J. Jaramillo, R. Gomperts, R. E. Stratmann, O. Yazyev, A. J. Austin, R. Cammi, C. Pomelli, J. W. Ochterski, P. Y. Ayala, K. Morokuma, G. A. Voth, P. Salvador, J. J. Dannenberg, V. G. Zakrzewski, S. Dapprich, A. D. Daniels, M. C. Strain, O. Farkas, D. K. Malick, A. D. Rabuck, K. Raghavachari, J. B. Foresman, J. V. Ortiz, Q. Cui, A. G. Baboul, S. Clifford, J. Cioslowski, B. B. Stefanov, G. Liu, A. Liashenko, P. Piskorz, I. Komaromi, R. L. Martin, D. J. Fox, T. Keith, M. A. Al-Laham, C. Y. Peng, A. Nanayakkara, M. Challacombe, P. M. W. Gill, B. Johnson, W. Chen, M. W. Wong, C. Gonzalez, and J. A. Pople, , *Gaussian 03, Revision B.04*. 2003, Gaussian, Inc.: Pittsburgh PA.
31. Espanol, P. and P. Warren, *Statistical-Mechanics of Dissipative Particle Dynamics*. Europhysics Letters, 1995. **30**(4): p. 191-196.
32. Espanol, P., *Hydrodynamics from Dissipative Particle Dynamics*. Physical Review E, 1995. **52**(2): p. 1734-1742.
33. Consolati, G., et al., *Free volumes and occupied volumes in oligomeric polypropylenglycols*. Europhysics Letters, 2001. **53**(4): p. 497-503.
34. ACDLabs/ChemSketch. 2003, Advanced Chemistry Development, Inc.: Toronto ON, Canada.
35. Sun, H., P. Ren, and J.R. Fried, *The COMPASS force field: parameterization and validation for phosphazenes*. Computational and Theoretical Polymer Science, 1998. **8**(1-2): p. 229-246.
36. Karttunen, M.V., I.; Lukkarinen, A., *Novel Methods in Soft Matter Simulations*. 2004, Berlin Heidelberg: Eds.; Springer-Verlag.

37. Geerlings, P., F. De Proft, and W. Langenaeker, *Conceptual density functional theory*. Chemical Reviews, 2003. **103**(5): p. 1793-1873.
38. Parr, R.G., *Density Functional Theory*. Annual Review of Physical Chemistry, 1983. **34**: p. 631-656.
39. Yang, W.T. and R.G. Parr, *Hardness, Softness, and the Fukui Function in the Electronic Theory of Metals and Catalysis*. Proceedings of the National Academy of Sciences of the United States of America, 1985. **82**(20): p. 6723-6726.
40. Pearson, R.G., *Chemical hardness and density functional theory*. Journal of Chemical Sciences, 2005. **117**(5): p. 369-377.
41. Biegler-Konig, F., *Calculation of atomic integration data*. Journal of Computational Chemistry, 2000. **21**(12): p. 1040-1048.
42. Biegler-Konig, F., J. Schonbohm, and D. Bayles, *Software news and updates - AIM2000 - A program to analyze and visualize atoms in molecules*. Journal of Computational Chemistry, 2001. **22**(5): p. 545-559.
43. Verlet, L., *Computer Experiments on Classical Fluids: I. Thermodynamical Properties of Lennard-Jones Molecules* Phys. Rev., 1967 **159** (98 ).
44. Fletcher, R., Reeves C. M., *Function minimization by conjugate gradients* British Computer Society, 1964. **7**(2): p. 149-154.
45. Warshel, A., *Quantum Mechanical Consistent Force Field (QCFF/PI) Method: Calculations of Energies, Conformations and Vibronic Interactions of Ground and Excited States of Conjugated Molecules*. Israel J. Chem., 1973. **11**(709).
46. Hwang, M.-J.S., T. P.; Hagler, A. T., *Derivation of Class II force fields. 2. Derivation and characterization of a Class II forcefield*. J. Amer. Chem. Soc., 1994. **116**: p. 2515-2525.
47. Forster, S. and T. Plantenberg, *From self-organizing polymers to nanohybrid and biomaterials*. Angewandte Chemie-International Edition, 2002. **41**(5): p. 689-714.
48. Jones, R.A.L.R., R. W., *Polymers at Surfaces and Interfaces*. 1999, Cambridge: Cambridge University Press.
49. Jones, R.A.L.R., R. W., *Soft Condensed Matter*. 2006, Oxford: Oxford University Press.
50. Klok, H.A. and S. Lecommandoux, *Supramolecular materials via block copolymer self-assembly*. Advanced Materials, 2001. **13**(16): p. 1217-1229.

51. Discher, D.E. and A. Eisenberg, *Polymer vesicles*. *Science*, 2002. **297**(5583): p. 967-973.
52. Hamley, I.W., *Nanoshells and nanotubes from block copolymers*. *Soft Matter*, 2005. **1**(1): p. 36-43.
53. Mecke, A., C. Dittrich, and W. Meier, *Biomimetic membranes designed from amphiphilic block copolymers*. *Soft Matter*, 2006. **2**(9): p. 751-759.
54. Acatay, K., et al., *Tunable, superhydrophobically stable polymeric surfaces by electrospinning*. *Angewandte Chemie-International Edition*, 2004. **43**(39): p. 5210-5213.
55. Wang, J.G., et al., *Liquid crystalline, semifluorinated side group block copolymers with stable low energy surfaces: Synthesis, liquid crystalline structure, and critical surface tension*. *Macromolecules*, 1997. **30**(7): p. 1906-1914.
56. M. Antonietti; Oestreich, S., Eds., *Fluoropolymers I: Synthesis*. 1999, NY: Plenum Press.
57. Krishnan, S., Y.J. Kwark, and C.K. Ober, *Fluorinated polymers: Liquid crystalline properties and applications in lithography*. *Chemical Record*, 2004. **4**(5): p. 315-330.
58. Furo, I., *NMR spectroscopy of micelles and related systems*. *Journal of Molecular Liquids*, 2005. **117**(1-3): p. 117-137.
59. Bernazzani, L., et al., *On the interaction of sodium dodecyl sulfate with oligomers of poly(ethylene glycol) in aqueous solution*. *Journal of Physical Chemistry B*, 2004. **108**(26): p. 8960-8969.
60. Desimone, J.M., et al., *Dispersion Polymerizations in Supercritical Carbon-Dioxide*. *Science*, 1994. **265**(5170): p. 356-359.
61. Kendall, J.L., et al., *Polymerizations in supercritical carbon dioxide*. *Chemical Reviews*, 1999. **99**(2): p. 543-563.
62. McClain, J.B., et al., *Design of nonionic surfactants for supercritical carbon dioxide*. *Science*, 1996. **274**(5295): p. 2049-2052.
63. Eastoe, J., et al., *Water-in-CO<sub>2</sub> microemulsions studied by small-angle neutron scattering*. *Langmuir*, 1997. **13**(26): p. 6980-6984.
64. Hoefling, T.A., R.M. Enick, and E.J. Beckman, *Microemulsions in near-Critical and Supercritical CO<sub>2</sub>*. *Journal of Physical Chemistry*, 1991. **95**(19): p. 7127-7129.

65. Sarbu, T., T. Styranec, and E.J. Beckman, *Non-fluorous polymers with very high solubility in supercritical CO<sub>2</sub> down to low pressures*. *Nature*, 2000. **405**(6783): p. 165-168.
66. Folk, S.L., J.M. DeSimone, and E.T. Samulski, *Cationic poly(dimethylsiloxane) surfactants: Synthesis, characterization, and aggregation behavior in dense carbon dioxide, fluorinated, and silicon-containing solvents*. Abstracts of Papers of the American Chemical Society, 2001. **221**: p. U346-U346.
67. Consani, K.A., Smith, D. R., *Observations on the solubility of surfactants and related molecules in carbon dioxide at 50°C*. *J. Supercrit. Fluids* 1990. **3**: p. 51-65.
68. *MATLAB*. 1994, The Mathworks Inc. : Natick, MA.
69. Lees, A.W., Edwards, S. F., *The computer study of transport processes under extreme conditions*. *J. Phys. C*, 1972. **5**: p. 1921-1929.
70. Baysal, C. and H. Meirovitch, *New conformational search method based on local torsional deformations for cyclic molecules, loops in proteins, and dense polymer systems*. *Journal of Chemical Physics*, 1996. **105**(17): p. 7868-7871.
71. Baysal, C. and H. Meirovitch, *Efficiency of the local torsional deformations method for identifying the stable structures of cyclic molecules*. *Journal of Physical Chemistry A*, 1997. **101**(11): p. 2185-2191.